A&A 566, A103 (2014)
DOI: 10.1051/0004-6361/201423497

Astronomy & Astrophysics

High-resolution imaging of *Kepler* planet host candidates

A comprehensive comparison of different techniques⋆

J. Lillo-Box, D. Barrado, and H. Bouy

Departamento de Astrofísica, Centro de Astrobiología (CSIC-INTA), ESAC campus, 28691 Villanueva de la Cañada, Madrid, Spain
e-mail: Jorge.Lillo@cab.inta-csic.es

Received 23 January 2014 / Accepted 29 April 2014

ABSTRACT

Context. The *Kepler* mission has discovered thousands of planet candidates. Currently, some of them have already been discarded; more than 200 have been confirmed by follow-up observations (most by radial velocity and few by other methods), and several hundreds have been validated. However, the large majority of the candidates are still awaiting for confirmation. Thus, priorities (in terms of the probability of the candidate being a real planet) must be established for subsequent radial velocity observations.
Aims. The motivation of this work is to provide a set of isolated (good) host candidates to be further tested by other techniques that allow confirmation of the planet. As a complementary goal, we aim to identify close companions of the candidates that could have contaminated the light curve of the planet host due to the large pixel size of the *Kepler* CCD and its typical PSF of around 6 arcsec. Both goals can also provide robust statistics about the multiplicity of the *Kepler* hosts.
Methods. We used the AstraLux North instrument located at the 2.2 m telescope in the Calar Alto Observatory (Almería, Spain) to obtain diffraction-limited images of 174 *Kepler* objects of interest. A sample of demoted *Kepler* objects of interest (with rejected planet candidates) is used as a control for comparison of multiplicity statistics. The lucky-imaging technique used in this work is compared to other adaptive optics and speckle imaging observations of *Kepler* planet host candidates. To that end, we define a new parameter, the blended source confidence level (BSC), to assess the probability of an object to have blended non-detected eclipsing binaries capable of producing the detected transit.
Results. We find that 67.2% of the observed *Kepler* hosts are isolated within our detectability limits, and 32.8% have at least one visual companion at angular separations below 6 arcsec. Indeed, we find close companions (below 3 arcsec) for the 17.2% of the sample. The planet properties of this sample of non-isolated hosts are revised according to the presence of such close companions. We report one possible S-type binary (KOI-3158), where the five planet candidates would orbit one of the components of the system. We also report three possible false positives (KOIs 1230.01, 3649.01, and 3886.01) due to the presence of close companions that modify candidate properties such that they cannot be considered as planets anymore. The BSC parameter is calculated for all the isolated targets and compared to both the value prior to any high-resolution image and, when possible, to observations from previous high-spatial resolution surveys in the *Kepler* sample.

Key words. techniques: high angular resolution – planets and satellites: fundamental parameters – binaries: visual

1. Introduction

The *Kepler* mission has provided more than 6000 planet candidates[1] (*Kepler* objects of interest, KOI) in its more than four years of almost continuous operation. The end of phase K1 operations of the mission (extrasolar planets search) is by contrast the starting point of a new phase, which is the systematic analysis of the immense database produced by the observatory. In particular, the validation of these planet candidates is the first step to obtain a large catalog of confirmed extrasolar planets that help us to understand the formation, properties, evolution and death of planetary systems. More than 200 *Kepler* planets have been confirmed so far, which still represents less than 5% of the total sample of candidates. Several techniques (such as radial velocity, light curve variations, or transit timing variations) have been used to that end. However, the large pixel size of the *Kepler* camera (around 4 × 4 arcsec), the broad point spread function (PSF) of the *Kepler* telescope (with a typical[2] full width at half maximum of $FWHM \approx 6.4$ arcsec), and the size of the aperture (typically 6–10 arcsec) used to extract the photometry implies the need for obtaining high-resolution images prior to applying these (somehow expensive and time-consuming) confirmation techniques. Exhaustive statistical analysis has also provided hundreds of validated planets (e.g. Rowe et al. 2014; Lissauer et al. 2014).

High-resolution imaging observations have been previously carried out in other planetary samples (apart from *Kepler* candidates) with interesting results, such as the cases of WASP-2, TrEs-2 and TrEs-4 (see Daemgen et al. 2009), where the properties of the confirmed planets were revised due to the presence of close companions detected by the lucky imaging technique. To date, there are four extensive works on the *Kepler* sample that use different high-resolution techniques in different wavelength ranges: speckle imaging in the optical range (Howell et al. 2011), adaptive optics in the near-infrared (Adams et al. 2012, 2013), adaptive optics in the optical (Law et al. 2013), and lucky

⋆ Tables 1, 3, 4, 7, and 11 are available in electronic form at http://www.aanda.org

[1] Around 3600 candidates have passed all *Kepler* requirements. http://exoplanetarchive.ipac.caltech.edu/cgi-bin/ExoTables/nph-exotbls?dataset=cumulative

[2] http://keplerscience.arc.nasa.gov/calibration/KSCI-19033-001.pdf

imaging in the optical range (our previous catalog presented in Lillo-Box et al. 2012).

These high-spatial resolution surveys are important for three main reasons: 1) ruling out the possibility of chance-aligned sources in specific configurations that could mimic a planetary transit (e.g. background eclipsing binaries); 2) improving the orbital and physical parameters of the transiting object by accounting for possible extra sources in the *Kepler* aperture; and 3) detecting possible bound companions forming S-type binary systems, where the planet orbits one of the components of the system and acts on the other as a gravitational perturber (see Kley 2010). These points are crucial in our understanding of planetary systems (formation and evolution) and are the first step of the confirmation of *Kepler* planets. Indeed, in some cases, these observations represent a key step in the statistical validation of very small planets (with a mass too low to be detected by current radial velocity instruments) as was the case of Kepler-37b (Barclay et al. 2013).

In the present work, we release a new sample of lucky imaging observations of *Kepler* candidates and provide the isolated sample of candidates observed in our previous release (Lillo-Box et al. 2012). These isolated *Kepler* objects of interest (hereafter KOIs) represent an excellent sample of candidates to be followed-up, given the very low probability of contamination of their *Kepler* light curves (Barrado et al. 2013). In Sect. 2, we describe the target sample, the observations and the reduction of the data. The sensitivity limits of the images are shown in Sect. 2.5. In Sect. 3 we provide an update of our previous survey and the sample of isolated KOIs in our entire lucky imaging dataset. Statistics on the number of detected companions are given in Sect. 3.2. The analysis of the high-resolution images in terms of quality and how they reduce the probability for a particular KOI to have blended eclipsing binaries is explained in Sect. 4.1. In the case of KOIs with detected close companions, we provide estimations in Sect. 4.2 on how the transit depth and the planetary radius are modified due to the presence of such additional sources. A useful and comprehensive comparison between the different high-resolution imaging surveys of *Kepler* candidates, using different techniques, is presented in Sect. 5, and conclusions are summarized in Sect. 6.

2. Observations and data reduction

2.1. Target selection

Among the different releases of *Kepler* planet host candidates (Borucki et al. 2011; Batalha et al. 2013; Burke et al. 2013), a sample of few hundred targets were selected to be observed with high spatial resolution imaging. The selection criteria were based on both the interests of the planets themselves and the observational limitation imposed by the instrument/telescope configuration. The latter restriction is given by the combination of the CAHA 2.2 m telescope and the AstraLux instrument, which provides detectability limits of $m_{\rm SDSSi} = 20$–21 mag in total exposure times of around 2700 s. Since we wanted to detect possible companions that are at least 5.0 mag fainter at 1.0 arcsec (fainter visual companions would usually not affect the planet-star properties significantly), the faintest targets that we observed were of $m_{\rm Kep} < 18$ mag. From a practical point, except in few exceptions, we avoided observing KOIs that are fainter than $m_{\rm Kep} = 16$ mag to ensure the significance of our results.

In total, we observed 230 KOIs (101 KOIs in 2011, already reported in Lillo-Box et al. 2012, with detailed information about 44 objects with possible companions, 21 KOIs in 2012, and 108 KOIs in 2013) hosting 376 planet candidates. Unfortunately, after some of these KOIs were observed, some of their hosted planet candidates were rejected for different reasons (re-analysis of the light curve by *Kepler* team, radial velocity observations, etc.). As a consequence, a total of 56 KOIs among our targets (including all but one of the KOIs with $m_{\rm Kep} > 16$) do not seem to host a planet candidate anymore. On the positive side, we have used these 56 demoted KOIs as sample control so that the same study was carried out for this sample. This leaves us with 174 planet host candidates in our sample (97 KOIs in 2011, 20 KOIs in 2012, and 57 KOIs in 2013) by hosting 313 planet candidates. Among these 174 KOIs, nine have all their candidates already confirmed[3]: KOI-0041 or Kepler-100, KOI-0069 or Kepler-93, KOI-0082 or Kepler-102, and KOI-1925 or Kepler-409 from Marcy et al. (2014), KOI-1529 or Kepler-59 (Steffen et al. 2012), KOI-0196 or Kepler-41 (Quintana et al. 2013), KOI-0351 or Kepler-90 (Cabrera et al. 2014), KOI-0245 or Kepler-37 (Barclay et al. 2013), KOI-0094 or Kepler-89 (Weiss et al. 2013), KOI-2133 or Kepler-91 (Lillo-Box et al. 2014), and KOI-0571 or Kepler-186 (Quintana et al. 2014).

2.2. Data acquisition and reduction

We applied the lucky imaging technique to the selected targets to achieve diffraction-limited resolution. We used the AstraLux North instrument located at the 2.2 m telescope at the Calar Alto Observatory (Almería, Spain). The targets were observed along three visibility windows of the *Kepler* field during 2011, 2012, and 2013. The results regarding the non-isolated KOIs of observations on 2011 were published in Lillo-Box et al. (2012). In the present work, we report the results concerning the isolated candidates observed in 2011 and the new results for the 2012–2013 observing runs.

We used exposure times for the single frames in the range 30–90 milliseconds (which is below the coherence time of the atmospheric turbulence) and set the number of frames accordingly to accomplish our depth requirement (typically 20 000–40 000 frames). In all cases, we used the full CCD array of the camera (24 × 24 arcsec). In the same line as in our previous work, this observing configuration ensures the aimed coverage both in contrast and angular separation from the main target. Table 1 lists the observing characteristics (date, individual exposure times, and number of frames) for each target.

Data cube images were reduced by using the online pipeline of the instrument (see Hormuth 2007), which performs basic reduction and selects the highest quality images. Then, it combines the best 1.0%, 2.5%, 5.0%, and 10% frames with the highest Strehl ratios (Strehl 1902). It calculates the shifts between the single frames, performs the stacking, and resamples the final image to have half the pixel size (i.e. around 0.023 arcsec/pixel). In this paper, we only use the 10% selection rate images (which we simply call AstraLux images). We chose this particular selection rate, since it provides the best compromise between a good angular resolution and the largest magnitude depth, according to our previous experience with the instrument and recommendations from Felix Hormuth (PI of the instrument).

2.3. Astrometric calibration

We acquired images of the M15 globular cluster in all three observing seasons to obtain the relative plate solution of the

[3] As for January 20th, 2014.

Table 2. Plate solution for our photometric observations (see Sect. 2.3).

Parameter	Units	2011	2012	2013
# stars		100	179	239
Pixel scale	mas/px	23.89 ± 0.23	23.89 ± 0.23	23.61 ± 0.20
PA	degrees	1.74 ± 0.54	1.94 ± 0.57	1.96 ± 0.50

CCD. We used the more than 100 cross-matched sources with the Yanny et al. (1994) catalog to obtain the plate scale and position angle of the CCD. We compared the angular separations and position angles of more than 1000 randomly selected star pairs in the latter catalog (separations in arcsec) and in our own catalog (separations in pixel units). The derived pixel size and position angle of the CCD for each observing season are shown in Table 2. We obtained typical uncertainties of 0.20 mas/px (around 1% of relative error) for the pixel size.

2.4. Source detection and photometry

Sources were identified in each image by using our semi-automatic routine specifically designed for the instrument. The algorithm first detects possible sources in the image whose integrated flux over an aperture of 10 pixels is, at least 3 times greater than the corresponding flux of the sky in the image (measured as the median value of all pixels, assuming that most of the image is not covered by stars). Then, each source candidate is individually checked to fulfill specific criteria, such as having a PSF-like radial profile shape (to reject possible artifacts and cosmic rays) or having magnitudes in the range of 0–30 to reject possible remaining bad pixels. All images were then manually inspected to check the final detected sources.

We then applied aperture photometry to measure the relative magnitudes between objects in the same image. We used the *aper* routine in IDL to extract the flux contained within a specified aperture. This aperture is selected for each image by taking the close objects in the field to avoid contamination of close companions into account. Thus, for each image, we have the instrumental magnitudes for all sources and the magnitude differences with respect to the KOI (which we call Δm). In cases where a close companion (below 3 arcsec) was found, we obtained additional photometry in the $z_{\rm AstraLux}$ filter (equal to the SDSSz filter from the Sloan Digital all-Sky Survey) to characterize the secondary object.

Absolute calibration was then performed by using the KIC photometry of the KOI and the instrumental magnitudes and magnitude differences of the surrounding objects with respect to the KOI. First, KIC magnitudes were converted to SDSS magnitudes by using the photometric transformations presented by Pinsonneault et al. (2012) in their Eqs. (3) and (4). According to Brown et al. (2011), the KIC images have a full width at half-maximum of 2.5 arcsec. Hence, as stated by the authors, the KIC photometry is unable to resolve the components of close binary stars. According to this, we can consider that their PSF photometry cannot resolve visual companions closer than 2.5 arcsec, so the magnitudes of such KOIs account for the flux of all sources inside such radius. Thus, we can distinguish between two cases to calibrate our photometry: KOIs with and without companions closer than 2.5 arcsec.

When any close companion was detected, we derived the photometric zeropoint of our Astralux images using the *i*-mag provided in the KIC, neglecting atmospheric or instrumental effects.

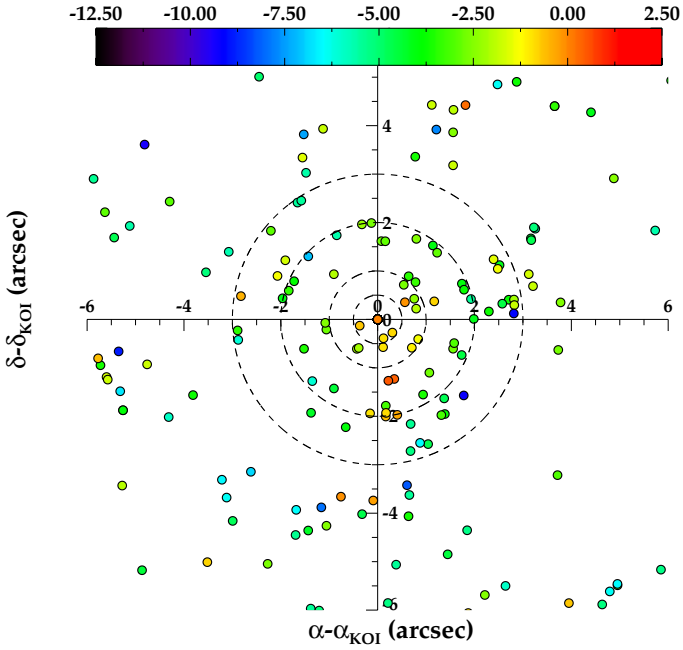

Fig. 1. Location of the detected companions to the KOIs in our sample. Each filled circle corresponds to a detected source and its relative position in the projected sky with respect to the KOI. The colors represent the magnitude difference between the companion and the corresponding KOI. We have marked with dashed circles the 0.5, 1.0, 2.0, and 3.0 arcsec separations for visualization purposes.

In the case where a close companion was found, we assume that the KIC magnitude that is converted to the SDSS system ($m_{\rm SDSS}$) is actually the sum of the fluxes coming from all sources inside 2.5 arcsec. If we call $\Delta m^j_{\rm AstraLux}$ to the magnitude difference of the jth object inside 2.5 arcsec from the KOI, as detected by AstraLux, the calibrated magnitude of the KOIs must read

$$m^{\rm KOI}_{\rm AstraLux,cal} = m_{\rm SDSS} + 2.5\log\left(1+\sum_{\rm j} 10^{0.4\Delta m^j_{\rm AstraLux}}\right). \quad (1)$$

Having the calibrated magnitude of the KOI, we can obtain the absolute magnitudes of all companions in the image as $m^{C/}_{\rm AstraLux,cal} = m^{\rm KOI}_{\rm AstraLux,cal} - \Delta m^{C/}_{\rm AstraLux}$, where $C/$ represents the values for the companion. This scheme was then applied to both filters i and z to obtain the absolute SDSS magnitudes of all objects detected in the images.

In Table 3, we provide the complete catalog of sources detected within 6 arcsec from the KOIs observed during 2012 and 2013. In Fig. 1, we show the location of all companions found within 6 arcsec for KOIs that are observed during our three observing seasons. The color-code in the figure shows the magnitude difference in the i filter. Figure 1 illustrates the high density of close visual companions and the need to obtain high resolution images of all candidates to better characterize the systems.

The identified isolated KOIs are studied in more detail in Sect. 4.1. These targets are thus suitable to proceed with radial velocity studies, since no objects have contaminated the *Kepler* light curve and cannot contaminate the radial velocity data within our sensitivity and detectability limits (presented in the next section).

2.5. Completeness, detectability, and sensitivity limits

In high-spatial resolution studies, it is crucial to determine the limitations of our images in terms of completeness, contrast, and how contrast depends on the separation to the main target. These three concepts completely describe the quality of the observation and, thus, should be individually calculated and reported for each image.

We refer to Lillo-Box et al. (2012) for a detailed explanation about the employed method to measure both the completeness and detectability magnitudes. In brief, we used three images with a total exposure time each of 200 s for the globular cluster M15 to compute these parameters. According to the detected sources in these images, we found the mean completeness value to be $i_{\rm complete} = 18.4 \pm 0.3$ mag and to reach detectability down to approximately $i_{\rm detect} = 21.7$ mag at 5σ level. Since different exposure times were set for each image and selection rate, we have to extrapolate these values individually. In particular, we have scaled the completeness and detectability limits for each particular object and selection rate by adding the quantity $-2.5\log(200\ {\rm s}/t_{\rm exp}(s))$ to the detectability and completeness magnitudes shown above. Here, $t_{\rm exp}$ is the effective exposure time of each image (i.e. the individual exposure time per frame multiplied by the number of selected and stacked frames). The resulting values are shown in Table 1 for each individual object.

The sensitivity limits (i.e. the faintest stars detectable in our images at each angular separation, which we also call sensitivity curve, $C_{\rm sens}$) were also determined for each image once the KOI was identified. We artificially add a similar PSF compared to the one of the main target but scaled by a factor of Δm (i.e. $F_2 = F_{\rm KOI}10^{-0.4\Delta m}$) at different positions of the image. We used 20 angular separations between $\alpha = 0.1$ and $\alpha = 3.0$ arcsec and 20 relative magnitudes (Δm) between 0 and 10 mag. For every pair $[d, \Delta m]$, we added ten artificial stars that are distributed at random angles (hence, 4000 artificial stars were included), and we run our detection algorithm used to detect the companion sources (see Sect. 2.4) to try detecting these artificially added companions. The sensitivity curve ($C_{\rm sens}$) is then computed as the contour line in the $[d, \Delta m]$ plane, which shows that at least 7 out of the 10 artificially added stars were detected with a 5σ minimum requirement for the detection. The sensitivity curve calculated for KOI-0082 is shown in Fig. 2 to illustrate the results and to compare other high-spatial resolution surveys to that also observed this target (a quantitative comparison of these studies for the coincident objects is performed in Sect. 5). The sensitivity limits at different angular separations for each KOI in this work are presented in Table 4 for the corresponding i and z filters.

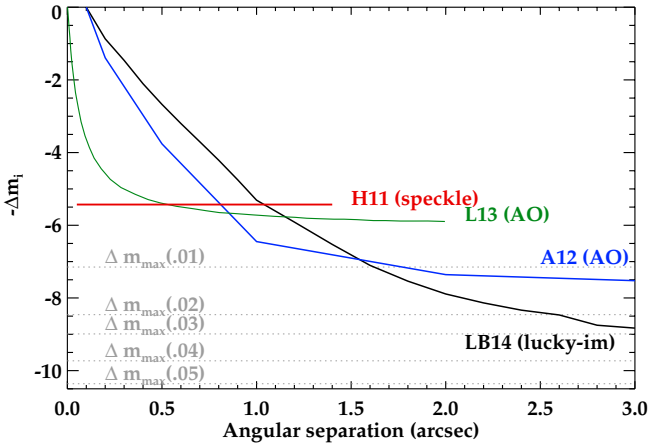

Fig. 2. Sensitivity limits ($C_{\rm sens}$) of KOI-0082 in the four main high-resolution imaging surveys in the *Kepler* sample, namely Howell et al. (2011), red solid line; Adams et al. (2012), blue solid line; Law et al. (2013), green solid line; and this work, LB14, black solid line. The horizontal grey dotted lines show the maximum magnitude difference that a companion should have to mimic the transit of every planet candidate in that system (see Eq. (2) and Sect. 4.1.1)

3. Results

In what follows, we use the isolated designation to those KOIs that do not present companions closer than 6 arcsec from the KOI. This limit comes from the typical values of the *Kepler* PSF, and the typical apertures used to extract the photometry, which ranges between 6–10 arcsec. Note that stars beyond the 6 arcsec limit would have been detected by more conventional surveys.

3.1. Update on 2011 results

In Lillo-Box et al. (2012), we observed 98 KOIs and concluded that 57 were actually isolated, 27 presented at least one companion between 3–6 arcsec, and 17 presented at least one companion closer than 3 arcsec. The new (more accurate) astrometric calibration presented in this paper with the update of the list of false positives implies that these numbers have slightly changed. The updated results for the 2011 observing season provide 63 isolated KOIs (65.0%), 22 KOIs with companions at 3–6 arcsec (22.7%), and 15 KOIs with companions closer than 3 arcsec (15.5%) out of 97 KOIs. (We removed those that currently do not present any planet candidate, namely KOI-0644, KOI-0703, and KOI-0465, and added other two not included in the previous analysis, namely KOI-0490 and KOI-0408.)

3.2. Results from the new sample

In this work, we add information about another 77 KOIs with active planet candidates (nine of them with all their transiting candidates already confirmed, see Sect. 2.1). Among this new sample, we find that 54 KOIs are isolated (70.1% of the new sample), and 23 KOIs (29.9%) have at least one companion closer than 6 arcsec (inside the typical *Kepler* PSF). Among the non-isolated KOIs, we find that 12 KOIs (15.6%) show at least one companion between 3–6 arcsec, and 15 KOIs (19.4%) show at least one object below 3 arcsec (which means that 4 KOIs present companions in both ranges). These numbers are relatively similar and consistent to those obtained in the 2011 run.

According to the updated numbers from the 2011 observing season and to the addition of the new sample, we find that 111 are isolated (67.2%), 35 present at least one companion between 3–6 arcsec (20.1%), and 30 have companions closer than 3 arcsec (17.2%), among the 174 KOIs observed with remaining planet candidates,. All these values are summarized in Table 5. These results imply that we have a 67.2% probability that a KOI is isolated, regardless of the possible biases related to the target selection. However, there is a non-negligible 32.8% probability that a companion object inside the typical *Kepler* PSF exists, thus contaminating the *Kepler* light curve and modifying the derived properties of any planet candidate.

Table 5. Multiplicity results.

Run	Observed	Isolated	3–6 arcsec	0.1–3 arcsec
2011 (update)	97	63 (65.0%)	22 (22.7%)	15 (15.8%)
2012+2013	77	54 (68.4%)	12 (15.6%)	15 (19.7%)
Total	**174**	**117 (67.2%)**	**34 (19.5%)**	**30 (17.2%)**

Notes. The table shows the number of KOIs with at least one companion closer than 3 arcsec and 3–6 arcsec and those without companions closer than 6 arcsec within our observational limitations (see Sect. 2.5) for each season. The lower separation limit of 0.1 arcsec is due to the minimum achievable resolution with AstraLux in optimum weather conditions.

4. Analysis

4.1. Isolated planet host candidates

Once the sensitivity limits (i.e. the sensitivity curve) have been calculated for the images of the isolated KOIs (Sect. 2.5), the relevant information to be supplied by our high-resolution observations is how well we can be assured that no blended background or foreground sources can contaminate the detected transit signal.

Generally, our high-resolution images can play an important role in the rejection of two false positive scenarios. Other configurations, such as hierarchical triples or grazing eclipses cannot be ruled out by high-spatial resolution images, but their occurrence probabilities are extremely low. First and most critical, specific configurations of a blended unassociated eclipsing binary can reproduce the detected planetary transit of the candidate. According to Morton & Johnson (2011, hereafter MJ11), this case is of particular importance for shallow transits (with apparent depths below 10^3 ppm), which should be the case of smaller planets. In Sect. 4.1.1, we deeply investigate and quantify how our high-resolution images can reduce the probability of such scenario being the responsible of the detected transit.

Secondly, even if the transiting object is actually eclipsing the target star, the mere presence of single blended sources not accounted for in the light curve analysis can importantly dilute the transit depth. As a consequence, the transiting object would seem smaller than it actually is. This scenario is discussed and quantified in Sect. 4.1.2.

4.1.1. Blended source confidenc: Rejection of background eclipsing binary scenarios

As stated in MJ11, the probability of having a blended eclipsing binary ($P_{\rm BB}$) inside the PSF of the KOI can be split into two factors: the probability of having a blended source ($P_{\rm BS}$) and the probability for that source to be an eclipsing binary with the appropriate configuration to produce the observed transit ($P_{\rm appEB}$). While the second factor only depends on the galactic latitude and magnitude of the KOI (see Eq. (14) in MJ11), the first factor can be observationally constrained to some extent with high-resolution images.

To assess the contamination probability, we define a new parameter, the blended source confidence level (BSC), as the observational level of confidence that no blended sources are located within a given angular separation to the host candidate. The BSC is evaluated as the complementary probability of having a blended object that could mimic the observed transit.

i. Probability of having a blended source

For a given KOI, we can calculate the maximum contrast (with respect to the measured flux) that a hypothetical blended EB must have to mimic a transit of fractional depth δ (see Eq. (7) in MJ11). This equation reads

$$\Delta m_{\rm max}^{\rm kep} = m_{\rm EB} - m_{\rm target} = -2.5\ \log_{10}(\delta). \quad (2)$$

This value is valid for the *Kepler* filter. Since we are working with the i band of the SDSS, we have to compute the magnitude conversion. If we use the KIC (*Kepler* Input Catalog) magnitudes, we can easily see that the *Kepler* and $i_{\rm SDSS}$ magnitudes are linearly correlated. Since the vast majority of our isolated candidates lie in the range $13.0 < m_K < 16.0$ (only 2 have $m_K < 13.0$), we have only used KOIs in this range to compute the linear coefficients. We obtain that

$$i_{\rm SDSS} = 0.947 \cdot m_K + 0.510.$$

The linear correlation goodness of this fit is $R^2 = 0.98$, which is acceptable enough for this work. Thus, we can estimate the constrast in the $i_{\rm SDSS}$ band as $\Delta i_{\rm SDSS} = 0.947 \cdot \Delta m_K$, so that

$$\Delta m_{\rm max}^{i_{\rm SDSS}} = 0.947 \cdot [-2.5\ \log_{10}(\delta)]. \quad (3)$$

For clarity, we refer to this maximum constrast in the $i_{\rm SDSS}$ band as $\Delta m_{\rm max}$. In Fig. 3, we show the sensitivity curves of two KOIs and the $\Delta m_{\rm max}$ line that marks the limit to be reached by observations that minimize the probability of existence of a non-detected blended source capable of mimicking the transit signal.

Let us now, as a first step, assume one particular KOI with a magnitude m_i (in the SDSS photometric system) at galactic latitude b. The expected number of stars within an angular separation r from our KOI and with magnitudes in the range $[m_i, \Delta m_{\rm max}]$ is given by

$$N(r, b, m_i, \Delta m_{\rm max}) = \int_{0''}^{r} 2\pi\alpha\rho(b, m_i, \Delta m_{\rm max})\mathrm{d}\alpha = \pi r^2 \rho(b, m_i, \Delta m_{\rm max}), \quad (4)$$

where $\rho(b, m, \Delta m)$ represents the number of stars per unit area (density of stars) and depends on the galactic latitude (b) of the target and the requested magnitude range ($[m, m + \Delta m]$). For small areas[4], this value can be interpreted as the probability for this area that contains one chance-aligned star within this magnitude range. In that case, we can define the probability of an object having one companion source within a certain magnitude range as $P_{\rm aligned} = N(r, b, m, \Delta m)$. This equation clearly shows that the probability of a chance-aligned source decays with the square of the angular separation as we approach to the star. Contamination sources above 3.0 arcsec could have been easily detected by photometric observations as dedicated to the *Kepler*

[4] With small area, we mean that it must be accomplished that $r < R_{\rm max}$ where $R_{\rm max}$ is the radius that provides a value of unity for Eq. (4), in that it accomplishes $\int_0^{R_{\rm max}} 2\pi\alpha\rho(b, m, \Delta m)\mathrm{d}\alpha = 1$. We note that all studied KOIs accomplish $R_{\rm max} > 3.0$ arcsec.

field (such as in Brown et al. 2011, or the UKIRT J-band survey observed and supplied by Phil Lucas[5]), or by photocenter centroid analysis of the *Kepler* images (see, for example, Batalha et al. 2010). Hence, in this work, we only take the 0.0–3.0 arcsec region into account.

We can now integrate $P_{\rm aligned}$ in the parameter space $\alpha = [0.0, 3.0]$ arcsec and $\Delta m = [0, \Delta m_{\rm max}]$ to compute the total a priori probability ($P_{\rm BS,0}$) for a particular target of magnitude m_K that contains a chance-aligned source with magnitude $m_i < m < m_i + \Delta m_{\rm max}$ within 3 arcsec:

$$P_{\rm BS,0} = \int_{0''}^{3''} 2\pi\alpha\rho(b, m_i, \Delta m_{\rm max})\, {\rm d}\alpha = 9\pi\rho(b, m_i, \Delta m_{\rm max}). \quad (5)$$

ii. Calculating the ρ parameter

We have calculated the density of stars parameter (ρ) for each planet candidate in a similar way as MJ11. We used the online tool TRILEGAL[6] to compute the number of expected stars with a limiting magnitude in a particular region of the sky. We used the default parameters for the bulge, halo, thin/thick disks, and the lognormal initial mass function from Chabrier (2001). As the *Kepler* field is relatively large and encompasses around 12 degrees in each direction (and almost 20 degrees in galactic latitude), we have found important differences in the stellar density from galactic latitudes that are close to the galactic disk to those farther from it. Due to the large number of targets in this paper and given that it is not possible to perform an automatic query in TRILEGAL (the user must proceed object by object), it is not possible to obtain individual populations for each target. Since the ρ parameter just depends on the galactic latitude, we obtained instead stellar populations for regions of 1 deg^2 centered at $b = 6°$ to $b = 22°$ in steps of 1° and a galactic longitude fixed to the center of the *Kepler* field (i.e. 76°), as seen in Fig. 4. We then simulate stars up to a magnitude limit of $i_{\rm SDSS} = 28$ inside each region according to the galactic model.

For a particular KOI at a galactic latitude $b_{\rm KOI}$ with a magnitude m_i and a needed depth in magnitude of Δm_i, we determine $\rho(b_{\rm j}, m_i, \Delta m_i)$ (j subscript representing each galactic latitude for which we run the TRILEGAL simulations) at all galactic latitudes in the grid by just counting stars within the magnitude range $[m_i, m_i + \Delta m_i]$ and dividing by the box area of 1 deg^2. Then we perform a low-order polynomial fit to the *rho* versus galactic latitude values and infer the corresponding $\rho(b_{\rm KOI}, m_i, \Delta m_i)$ by evaluating the fitted function at $b_{\rm KOI}$. We found that a polynimial of order five fits the data sufficiently well for the purposes of this work (see the example in Fig. 5). By following this scheme, we can precisely estimate the density of stars in a concrete magnitude range at any position in the *Kepler* field.

iii. Observing constraints and the BSC parameter

In Sect. 4.1.1, we have described how we define the probability of having a blended source within some observational constraints (namely, the star position and the magnitude range of possible blended stars). Since we have calculated a sensitivity line for each observation, we can reduce the a priori probability ($P_{\rm BS,0}$) by limiting this calculation to only that region where our image is not sensitive. In the angular separation versus magnitude difference plane, this non-sensitive zone is defined as the region between our sensitivity curve ($C_{\rm sens}$) and the maximum magnitude difference of a possible blended eclipsing binary that could mimic our transit signal ($\Delta m_{\rm max}$). In Fig. 3, this region has been shaded with diagonal lines. Hence, with the CAHA/AstraLux high-resolution observations, the probability

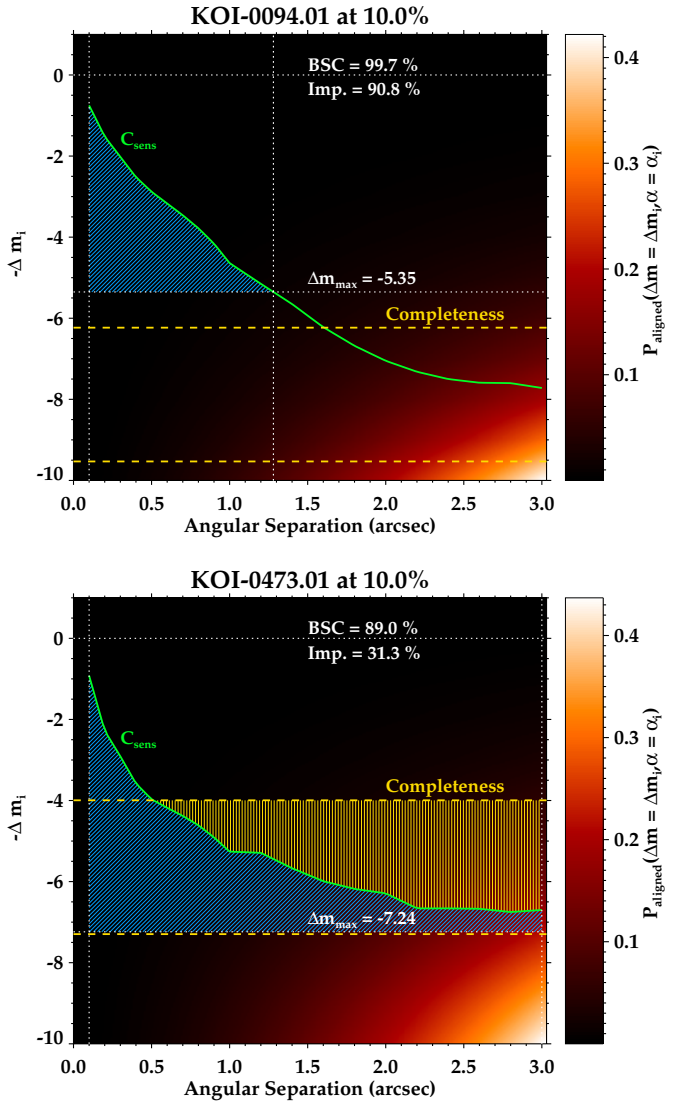

Fig. 3. Example of the determination of the BSC parameter (see Sect. 4.1.1) for two KOIs with conclusive (top panel) and non-conclusive (*bottom panel*) results. The green solid line represents the 5σ sensitivity limit (or sensitivity curve, $C_{\rm sens}$) for the CAHA/AstraLux image (calculated as explained in Sect. 2.5). The lower horizontal dotted white line represents the maximum magnitude difference $\Delta m_{\rm max}$ of a possible eclipsing binary that could mimic the transit signal as expected for these KOIs (see Sect. 4.1.1). The two vertical white dotted lines show the lowest angular separation detectable in the image (left line) and the intersection between the sensitivity curve and the $\Delta m_{\rm max}$ (right line). The upper and bottom dashed yellow lines represent the completeness and detectability levels (respectively) for the given KOI. The incompleteness region is marked in the *bottom panel* by the dashed region with vertical yellow lines. The uncovered region is shadowed with diagonal light blue lines. The background color code in the image represents the probability of having a chance-aligned background source for every angular separation and magnitude difference for the given KOI. The first example corresponds to excellent data (deep enough so that no incomplete region is present), whereas the second example is not deep enough. The $\Delta m = 0$ is marked by the upper horizontal dotted line.

[5] See http://keplergo.arc.nasa.gov/ToolsUKIRT.shtml
[6] http://stev.oapd.inaf.it/cgi-bin/trilegal

Table 6. Multiplicity results for the four main works on high-resolution imaging on the *Kepler* sample of candidates.

Targets with remaining planet candidates (current valid KOIs)							
Study	Technique[a]	Observed	Isolated	0.0″–1.4″	0.0″–2.5″	0.0″–3.0″	3″–6″
Howell et al. (2011)	speckle, opt	131	—	4 (3%)	—	—	—
Adams et al. (2012, 2013)	AO, near-IR	85	37 (44%)	12 (14%)	23 (27%)	28 (33%)	30 (35%)
Law et al. (2013)	AO, opt	697	—	29 (4%)	49 (7%)	—	—
Lillo-Box et al. (2012, 2014)	lucky, opt	174	117 (67%)	9 (5%)	25 (14%)	30 (17%)	34 (20%)
All targets observed (valid and demoted KOIs)							
Study	Technique[a]	Observed	Isolated	0.0″–1.4″	0.0″–2.5″	0.0″–3.0″	3″–6″
Howell et al. (2011)	speckle, opt	155	—	9	—	—	—
Adams et al. (2012, 2013)	AO, near-IR	101	45	16	28	34	36
Law et al. 2013	AO, opt	714	—	31	51	—	—
Lillo-Box et al. (2012, 2014)	lucky, opt	234	154	14	36	43	48
Demoted KOIs							
Study	Technique[a]	Observed	Isolated	0.0″–1.4″	0.0″–2.5″	0.0″–3.0″	3″–6″
Howell et al. (2011)	speckle, opt	24	—	5	—	—	—
Adams et al. (2012, 2013)	AO, near-IR	16	8	4	5	6	6
Law et al. (2013)	AO, opt	17	—	2	2	—	—
Lillo-Box et al. (2012, 2014)	lucky, opt	56	38	5	11	13	13

Notes. We show the number of detected companions for different separation ranges. The lower part of the table shows the statistics regardless whether the KOI still hosts planet candidates. We have 56 KOIs that have been demoted in the latest *Kepler* releases and are not classified as planet hosts any longer. In the case of Howell et al. (2011), there are 24 demoted KOIs, there are 16 for Adams et al. (2012, 2013), and there are 17 for Law et al. (2013). These results are presented int the third section of this table. [(a)] Technique and wavelength range (opt = optical, near-IR = near-infrared) used in the study.

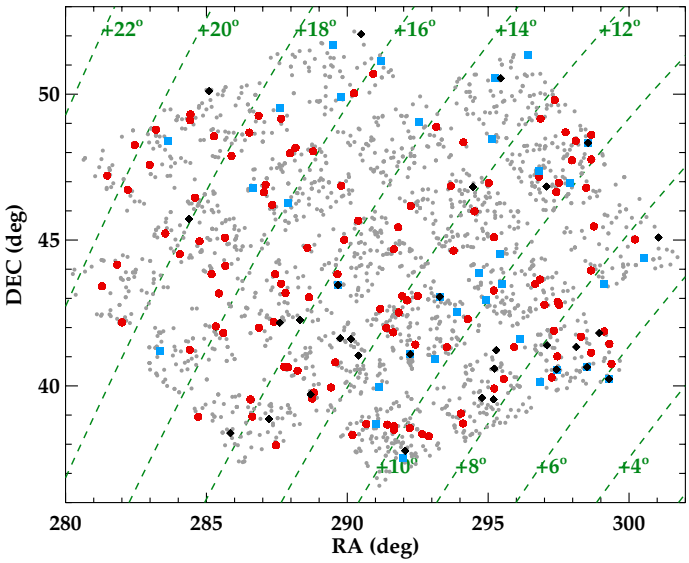

Fig. 4. Location of the isolated KOIs (red circles), KOIs with companions at 3–6 arcsec (blue squares), and KOIs with detected companions closer than 3 arcsec (black diamonds), as detected by the CAHA/AstraLux survey. Planet candidates from Batalha et al. (2013) are plotted as grey small circles. Iso-galactic latitude lines are marked as dashed inclined green lines parallels to the galactic plane.

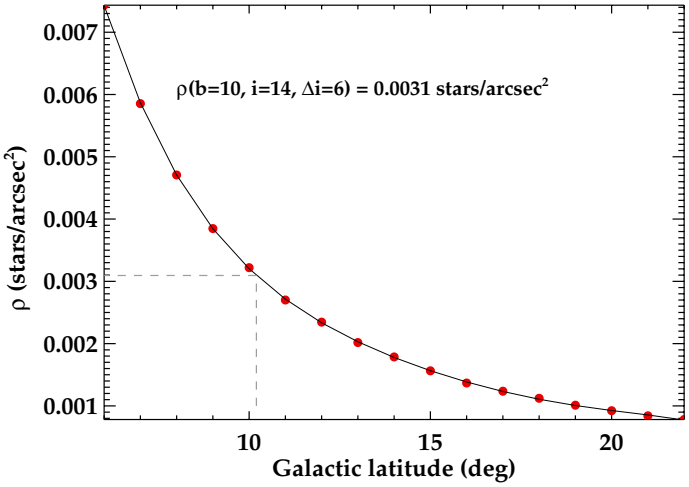

Fig. 5. Example of the determination of the ρ parameter for an object at b = 10 deg with a required magnitude range of i = 14–20 mag. Red filled circles represent the values for each galactic latitude in Fig. 4 (i.e. the $\rho[b, m_i, \Delta m_i]$ with b ranging from 6° to 22°), and the solid black line shows the correspoding five-degree polynomial fit. Gray dashed lines show the derived value at the requested galactic latitude in the example.

is given by Eq. (5) but now integrates only over the diagonally shaded region:

$$P_{\rm BS} = P_{\rm BS,0} - \int_{0''}^{3''} 2\pi\alpha \times \rho[b, m_i, \Delta m_0(\alpha)]\, {\rm d}\alpha, \quad (6)$$

where $\Delta m_0(\alpha) = max[C_{\rm sens}(\alpha), \Delta m_{\rm max}]$ and the second term in the right hand side of the expression represents the contribution of the high-resolution image.

It is thus clear that the better and deeper our image (i.e. the closer $C_{\rm sens}$ is to $\Delta m_{\rm max}$), the more we diminish the blended source probability and thus improve the planetary candidacy. We can now determine an observational value of $P_{\rm BS}$ and define the BSC parameter as BSC = 1 − $P_{\rm BS}$, representing the confidence for this source by not having blended eclipsing binaries mimicking the planetary transit. We propose this parameter to be used in all high-resolution studies to compare the different surveys with the adaptive optics, speckle, or lucky-imaging techniques. In column six of Table 7, we show the updated values of the $P_{\rm BS}$

according to our AstraLux observations (hereafter called $P_{\rm BS}^{\rm LB14}$ in %) for the isolated targets.

As an example, we obtain BSC = 99.5% in the upper panel of Fig. 3, given our high-resolution image of the planet host KOI-0094 and for its KOI-0094.01 planet candidate. In other words, there is a small probability (lesser than 0.5%) that we are missing a background source with the right magnitude to mimic the planetary transit ($P_{\rm BS} < 0.5\%$). It must be remembered that the $P_{\rm BS}$ probability must be multiplied by the probability of that source being an appropriate eclipsing binary ($P_{\rm appEB}$). This value, as calculated with the correlation explained in Eq. (14) in MJ11, is shown for each planet in the eighth column of Table 7.

iv. Corrections to the BSC due to incompleteness

In the bottom panel of Fig. 3, we can see an example of an image providing poor quality information. It is the case of KOI-0473. In this case, we have to make a correction to the BSC value because the completeness limit of our observation (corresponding to $i_{\rm complete}$, see Sect. 2.5) is above the sensitivity curve. Since the detectability limit ($i_{\rm detect}$) is below the sensitivity curve (i.e. $i_{\rm KOI} + \Delta m_{\rm max} < i_{\rm detect}$), we still could detect a percentage of sources with magnitudes above the completeness magnitude but not the all of them. Thus the contribution of the vertically shaded region (which we call incompleteness region, Incomp.Reg. in Eq. (7)) must be weighted by a function of the magnitude difference according to the decay in the probability detection. This function can be calculated by fitting the decay of the distribution of detected sources in the M15 images to an exponential function like $f(\Delta m) = C + A{\rm e}^{-\Delta m/B}$, where $\Delta m = m - m_{\rm complete}$. We can appropriately set $C = 0$ and $A = 1$, so that $f(\Delta m = 0.0) = 1.0$. From the M15 data (see Sect. 2.5), we derived the value $B = 0.667$. Thus, in the cases where the completeness line (upper yellow dashed line in Fig. 3) lies above the sensitivity curve ($C_{\rm sens}$, green line), the $P_{\rm BS}$ must be calculated as

$$P_{\rm BS}^{\rm corr} = P_{\rm BS,0} - \int_{r_0}^{3''} 2\pi\alpha\rho[b, m_i, \Delta m_1(\alpha)]\,{\rm d}\alpha + \int_{r_0}^{3''} {\rm d}\alpha \times \int_0^{\Delta' m(\alpha)} 2\pi\alpha\rho[b, m_{\rm comp}, \Delta m_2(\alpha)]\,{\rm e}^{\frac{-\Delta m_2(\alpha)}{B}}\,{\rm d}\Delta' m, \quad (7)$$

where

$$\Delta m_1(\alpha) = \max[m_i + C_{\rm sens}(\alpha), m_i + \Delta m_{\rm max}, m_{\rm comp}] - m_i \quad (8)$$

$$\Delta m_2(\alpha) = \max[m_i + C_{\rm sens}(\alpha), m_i + \Delta m_{\rm max}] - m_{\rm comp} \quad (9)$$

and r_0 represents the angular separation at which $m_i + C_{\rm sens}(\alpha = r_0) = m_{\rm comp}$. The second term corresponds to the contribution of the high-resolution image in the magnitude range where it is complete (non-shaded region above the $C_{\rm sens}$ line in Fig. 3). The third term represents the weightned contribution of the high-resolution image according to our exponential incompleteness function derived above, and it is represented by the vertically shaded region in the bottom panel of Fig. 3.

The results for KOI-0473.01 are worse than for KOI-0094.01, since we obtain a BSC parameter of 84.9% here, indicating that the depth of the image is less than what was needed for this particular object.

We have calculated the $P_{\rm BS}^{\rm LB14}$ parameter for all KOIs without companions closer than 3 arcsec. The results are presented in Col. 6 of Table 7. In this table, we also show the $P_{\rm BS,0}$ value (Col. 5) and the corresponding *improvement* obtained with our high-resolution observations (Col. 7). These values allow us to compare the quality of different high-resolution imaging techniques.

4.1.2. Rejecting diluted single-star scenarios

The second scenario that our high-resolution images can rule out is the case in which the presence of single-blended stars can dilute the transit depth of the eclipsing object so that it could mimic a planetary eclipse. Let us start with the simple case of one single star blended in the *Kepler* aperture. The observed transit depth can be calculated as $\delta = (F_{\rm nt} - F_{\rm t})/F_{\rm nt}$, where $F_{\rm nt}$ represents the measured flux when the object is not passing in front of the target star and $F_{\rm t}$ represents the flux when it is transiting the star. In the case of one single star contributing with a flux F_2 and the target star contributing with a flux F_1, we have $F_{\rm nt} = F_1 + F_2$ and $F_{\rm t} = F_1(1 - \epsilon)$, where ϵ is the actual fraction of the star covered by the transiting object and its value can be easily demonstrated to be equal to the true transit depth (i.e. $\epsilon = \delta_{\rm true}$). By using this, we can correct the transit depth due to the presence of a blended source as

$$\delta^{\rm true} = \delta^{\rm obs}\left(1 + 10^{-\Delta m/2.5}\right)^{1/2}, \quad (10)$$

where $\Delta m = m_2 - m_1$ represents the magnitude difference between the blended (m_2) and the target star (m_1) in the *Kepler* band. At this point, as stated by Law et al. (2013), we can distinguish between two cases: A) the transited star is brighter than the blended star ($\Delta m > 0$); and B) the transited star is fainter than the blended star ($\Delta m < 0$). To get the true radius of the transiting object, case B requires some knowledge about the radius ratio between the two stars involved. This requires additional knowledge of both stars (which means more free parameters rather than just the magnitude difference), which is out of the scope of this theoretical analysis.

In case A, however, assuming that the transit depth is releated to the radius ratio between the transiting object and the parent star as $\delta = (R_{\rm p}/R_\star)^2$, the true radius of the transiting object is given by

$$R_{\rm p}^{\rm true} = R_{\rm p}^{\rm obs}\left(1 + 10^{-\Delta m/2.5}\right)^{1/2}. \quad (11)$$

According to the most updated catalog of confirmed exoplanets[7], the empirical maximum possible radius for a planet is $R_{\rm p}^{\rm max} \approx 2.2\,R_{\rm J}$. Thus, we can calculate the maximum magnitude difference $\Delta m_{\rm max}^{\rm dil}$ that the blended source can have (i.e. how faint could it be) to dilute the transit depth, such that a non-planetary object (i.e. $R_{\rm p} > R_{\rm p}^{\rm max}$, regardless of its nature) appears as the true planet-size object:

$$\Delta m_{\rm max}^{\rm dil} = -2.5\log\left[\left(\frac{R_{\rm p}^{\rm max}}{R_{\rm p}^{\rm obs}}\right)^2 - 1\right]. \quad (12)$$

This equation indicates that the presence of undetected blended objects with magnitudes $m_1 < m_2 < m_1 + \Delta m_{\rm max}^{\rm dil}$ can dilute the transit depth of a non-planetary object down to that of a planetary object. According to this expression, case A only applies to candidates with $R_{\rm p}^{\rm obs} > 1.56\,R_{\rm J}$. In our sample, we only have six objects with $1.56\,R_{\rm J} < R_{\rm p}^{\rm obs} < 2.20\,R_{\rm J}$ (namely, KOI-0338.01, 1353.01, 1452.01, 2481.01, 3728.01, and 3765.01). For those

[7] We have checked the radii of the radial velocity confirmed extrasolar planets provided by The Extrasolar Planet Encyclopaedia (http://exoplanet.eu).

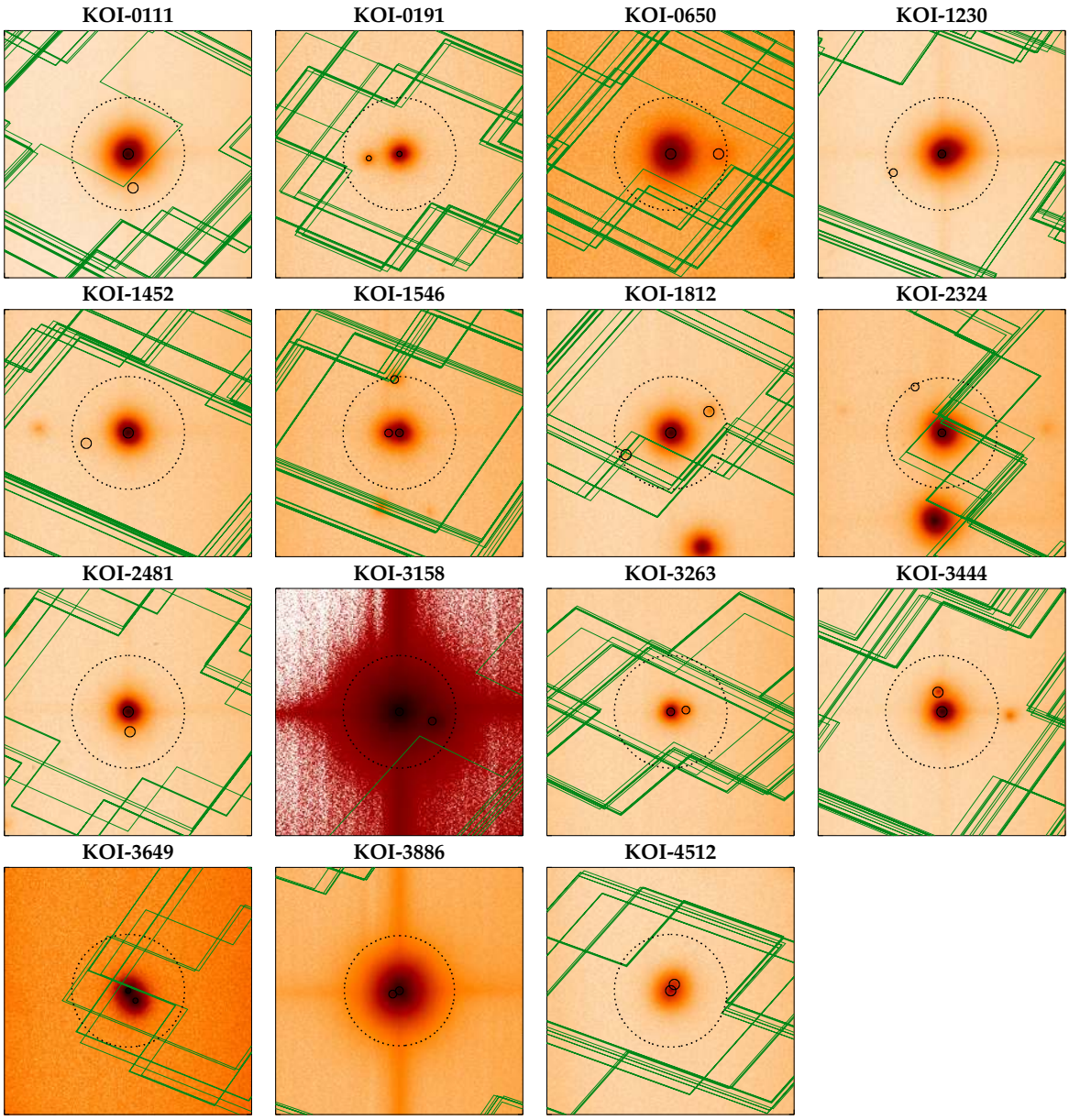

Fig. 6. High-resolution images obtained with AstraLux/CAHA of the 15 KOIs with detected companions closer than 3 arcsec. The dotted circles represent the 3 arcsec angular separations and the solid line circles show location of the detected sources. A color version of this figure can be found in the online version of the paper.

cases, we can proceed exactly as we did for the blended eclipsing binary scenario to get the $P_{\rm BS}$, but now we use $\Delta m_{\rm max}^{\rm dil}$ as the maximum magnitude value to get the probability of the presence of a diluter source $P_{\rm DS}$. The results show that this probability is dimminished from $P_{\rm DS,0} = 10^{-3}$–10^{-2} to $P_{\rm DS}^{\rm LB14} = 10^{-5}$–$10^{-4}$. Although the starting probabilities were already small, our high-resolution images showing no blended sources within our detection limits practically discard this possibility as a false positive scenario for these candidates.

We note that due to the mathematical shape of Eq. (12), we cannot perform this calculation for planet candidates with $R_{\rm p}^{\rm obs} > R_{\rm p}^{\rm max}$ (36 in our sample). Also, as stated by Law et al. (2013), case B would only affect few planet candidates with observed radii close to the limit $R_{\rm p}^{\rm obs} \approx 1.56\,R_{\rm J}$ and present blended stars with very small radius. Candidates with a small calculated radius are not affected by this scenario, although the presence of blended sources can modify their properties as we show in Sect. 4.2.1.

For cases with more than one blended star, the $P_{\rm DS}$ probability is insignificant for case A, since the probability of having two or more undeteced sources within our sensitivity limits is far smaller.

4.2. Non-isolated KOIs

We have found close companions (below 3 arcsec) for 15 KOIs among the sample of targets in the 2012 and 2013 observing seasons (see Fig. 6). The mere presence of such objects affects both the KOI status as a planet candidate and (if confirmed by other techniques) the derived planet properties, such as planet radius or impact parameter. Thus, the light curves of these targets should be studied in more detail, taking this additional sources into account. In Table 3, we provide the list of KOIs with companions below 6 arcsec. Among them, 15 KOIs present close companions (below 3 arcsec) that should be added to the 17 KOIs with detected sources by Lillo-Box et al. (2012).

Among the 15 KOIs with close companions, we obtained photometry in the z_{SDSS} band for five of them. In these cases, we can compute the $i - z$ color as

$$(i - z)_{/C} = \Delta i - \Delta z + (i - z)_{KOI}, \quad (13)$$

where the subscript $/C$ denotes that the value corresponds to the companion source and $\Delta i = i_{/C} - i_{KOI}$ and $\Delta z = z_{/C} - z_{KOI}$. By following the prescriptions described in Lillo-Box et al. (2012), we can estimate the spectral types of the objects by having the $i - z$ color information. For those without the z magnitude (mostly KOIs with companions at 3–6 arcsec), we searched for photometric information in public catalogs by using the last version of the Virtual Observatory SED Analyzer (Bayo et al. 2008, 2013, and in prep.). In cases where more than five photometric points are found, this tool fits a SED model to obtain the effective temperature of the source. Table 3 (Col. 10) shows the results for the sources for which this study was possible.

4.2.1. Effect on the planet properties

The diluted light from the blended companion that is not accounted in the light curve analysis provides erroneous determinations of the properties of the transiting object. We note that *Kepler* light-curves are deblended from sources detected by either the UKIRT J-band survey or by the KIC photometric survey on the *Kepler* field. Among the 15 KOIs with detected companions that are closer than 3 arcsec by the present survey, two of them have all their companions detected by the UKIRT J-band survey (namely KOI-0650 and KOI-1452). Thus, we can remove this KOIs from the current study. In the other two cases (KOI-1546 and KOI-1812), only one out of the two detected companions within 3 arcsec have also been detected by the UKIRT J-band survey. Thus, for these two, we only take the non-detected source into account. Finally, there are another two cases (KOI-2324 and KOI-3886), where the detection of the companions in the UKIRT J-band survey and their correspondence to our detected companions remains unclear. In what follows, we proceed for these targets as if their companions were non-detected by the UKIRT J-band survey. In total, 13 KOIs hosting 24 planet candidates are affected by additional non-accounted fluxes of blended companions.

In Sect. 4.3 of Lillo-Box et al. (2012) and Sect. 4.1.2 of this paper, we provided theoretical estimations of how the planetary radius of KOIs with detected close companions change because of the detection of blended stars (assuming the brighter object as the host star). In this work, we proceed in the same manner to estimate the corrected planetary radius. The results for the 24 affected planets in the 2012 and 2013 observed targets are listed in Table 8. The estimations clearly show the increase in the planetary radius caused by the non-accounted flux of the blended star. In three cases (namely, KOI-1230.01, KOI-3649.01, and KOI-3886.01), the planet candidate has a new estimated radius that according to mass-radius relations by Chabrier & Baraffe (2000) would yield to a typical mass of the transiting object in the stellar regime. We also note that the largest extrasolar planets confirmed so far[8] have a maximum radius below 2.2 R_j. Thus, we can flag these candidates as probable false positives.

We note that other orbital parameters, such as the semi-major axis or the impact parameter, are also affected by the presence of blended stars. However, the correction in these cases as well as a fine correction of the planetary radius involves careful re-analysis of the transit signals, which is out of the scope of this work.

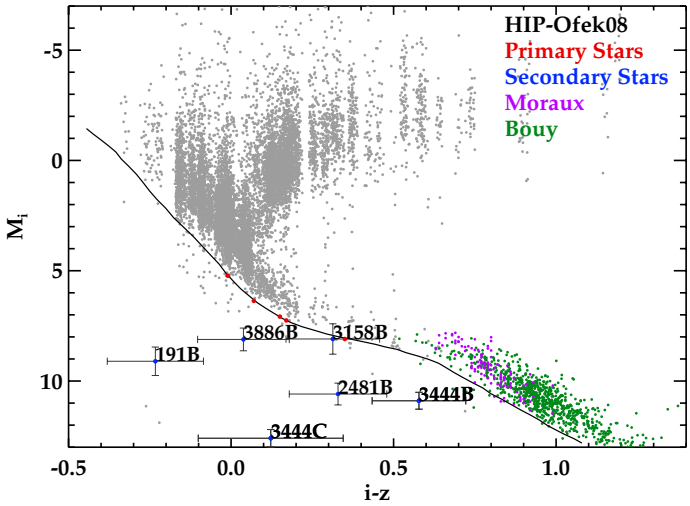

Fig. 7. Estimation of the possible bond of the close companions to KOIs detected in both i and z filters during the 2012 and 2013 observing seasons (see Sect. 4.2.2). The primary sources are represented in red and the close companions in blue. The solid black line represents the empirical ZAMS obtained by using the synthetic iz photometry from Ofek (2008) as grey dots, the observed members of the Pleiades cluster by Moraux et al. (2003) as purple circles, and Bouy et al. (2013) as green circles.

4.2.2. Physical bond of blended companions

For those KOIs with observations in both i and z filters, we can further constrain whether the close companions are bound or not to the central object using the color information. We proceed in the same way as in Lillo-Box et al. (2012, Sect. 4.2.2) by testing whether the close companions lie in the same zero-age main-sequence (ZAMS) as the central objects by projecting them to the same distance (see details in the aforementioned paper). Figure 7 summarizes the results for the five KOIs with remaining planet candidates and i, z observations during the 2012–2013 observing seasons. Among them, the companion to KOI-3158 (called KOI-3158B) seems to have a consistent age (within the uncertainties) with the main object, since they lie in the same ZAMS. This result agrees with a common formation of the two components, thus being a possible bound binary system. If this were the case, the estimated projected distance between the two components[9] would be 1100 ± 1000 AU for KOI-3158AB. According to our spectral type analysis based on the $i - z$ measured color in Sect. 4.2, the compainon is a redder object in the range K5-M1 (assuming that it is a main-sequence star).

Although the orbital parameters must be revised to account for the detection of the blended object, we can conclude that KOI-3158 is a potential candidate to be a S-type planetary systems. Indeed, it has five planet candidates as detected by *Kepler*.

According to their position in the Hertzprung-Russell diagram of Fig. 7, the remaining close companions (KOI-0191B, KOI-3886B, KOI-2481B, and KOI-3444C) are probably background sources.

[8] According to http://exoplanet.eu

[9] Obtained by assuming the distance to the KOI derived when the primary object is located in the empirical ZAMS. We obtain d = 600 ± 610 pc for KOI-3158.

Table 8. Estimation of the new parameters of the planet candidates orbiting the KOIs with detected companions closer than 3 arcsec.

Planet candidate	Cat.Depth ppm	New.Depth ppm	cat. R_p/R_s $\times 10^{-2}$	new R_p/R_s[a] $\times 10^{-2}$	sec R_p/R_s[b] $\times 10^{-2}$	Cat. R_p[c] $R_\oplus$	New R_p[d] $R_\oplus$
111.01	496	497.3 ± 1.7	2.107 ± 0.020	2.2301 ± 0.0038	43 ± 28	2.14	2.26
111.02	455	456.2 ± 1.6	2.024 ± 0.023	2.1359 ± 0.0036	41 ± 26	2.05	2.16
111.03	598	599.6 ± 2.0	2.328 ± 0.026	2.4487 ± 0.0042	47 ± 30	2.36	2.48
111.04	56	56.15 ± 0.19	0.76 ± 0.11	0.7493 ± 0.0013	14.5 ± 9.3	0.77	0.76
191.01	14 611	32 000 ± 5800	11.520 ± 0.051	17.9 ± 1.6	16.4 ± 1.2	11.00	17.10
191.02	664	1450 ± 260	2.426 ± 0.036	3.82 ± 0.34	3.49 ± 0.26	2.30	3.62
191.03	194	425 ± 77	1.291 ± 0.043	2.06 ± 0.19	1.89 ± 0.14	1.24	1.98
191.04	659	1440 ± 260	2.402 ± 0.073	3.80 ± 0.34	3.48 ± 0.26	2.30	3.64
1230.01	6998	6998 ± 17	8.259 ± 0.018	8.366 ± 0.010	700 ± 6100	37.10	37.58
1546.01	14 150	19 568 ± 79	10.624 ± 0.084	13.989 ± 0.028	22.61 ± 0.12	9.50	12.51
1812.01	1258	1277.8 ± 4.1	4.053 ± 0.065	3.5746 ± 0.0058	28.5 ± 2.9	4.80	4.23
2324.01[e]	149	149.39 ± 0.66	1.10 ± 0.46	1.2222 ± 0.0027	24 ± 21	0.32	0.36
2481.01	793	820 ± 12	2.750 ± 0.072	2.865 ± 0.021	15.3 ± 3.3	20.60	21.46
3158.01	26	56.8 ± 10.0	0.47 ± 0.12	0.753 ± 0.066	0.707 ± 0.055	0.30	0.49
3158.02	43	91 ± 16	0.73 ± 0.11	0.959 ± 0.084	0.900 ± 0.070	0.47	0.62
3158.03	48	103 ± 18	0.63 ± 0.12	1.017 ± 0.089	0.954 ± 0.074	0.41	0.66
3158.04	52	111 ± 20	0.65 ± 0.28	1.055 ± 0.093	0.990 ± 0.077	0.42	0.68
3158.05	73	157 ± 28	0.78 ± 0.14	1.25 ± 0.11	1.178 ± 0.091	0.51	0.81
3263.01	23 226	26 485 ± 95	16.88 ± 0.99	16.274 ± 0.029	43.44 ± 0.56	7.00	6.75
3444.01	199	219.6 ± 6.9	1.59 ± 0.77	1.482 ± 0.023	4.64 ± 0.72	1.04	0.97
3444.02	3285	3620 ± 110	8.8 ± 4.9	6.017 ± 0.095	18.9 ± 2.9	5.74	3.93
3444.03	96	105.8 ± 3.3	0.96 ± 0.49	1.028 ± 0.016	3.22 ± 0.50	0.63	0.67
3649.01	110 642	1 301 000 ± 41000	44.6 ± 2.7	114.1 ± 1.8	34.774 ± 0.050	65.36	167.18
3886.01[e]	441	1350 ± 300	1.86 ± 0.12	3.68 ± 0.41	2.56 ± 0.14	25.38	50.31
4512.01	3989	5954 ± 53	5.68 ± 0.00	7.717 ± 0.034	10.994 ± 0.099	6.19	8.41

Notes. [(a)] New planet-to-star radii ratio assuming no limb-darkening. [(b)] Planet-to-star radius assuming that the host is actually the secondary companion detected at less than 3 arcsec. [(c)] Planet radii calculated by the *Kepler* project (http://exoplanetarchive.ipac.caltech.edu) [(d)] Planet radii assuming the new depth and no limb-darkening. Please note that this could be the cause that the new derived radii are smaller than catalog radii in some cases. No error is presented since no error in the stellar radii is given. [(e)] According to the UKIRT *J*-band catalog of the *Kepler* field, it remains unclear to us if the detected companions to these KOIs in this paper match some of the targets in the UKIRT catalog.

4.3. A control sample: demoted KOIs

As was mentioned in Sect. 2.1, 56 KOIs were rejected as candidates after our lucky-imaging observations were performed (and we call them demoted KOIs). We have taken profit of these observations to contrast the multiplicity results. Among the demoted KOIs, we have found that 38 (67.8%) are actually isolated; 5 (8.9%) present one source closer than 1.4 arcsec; 11 (19.6%) present at least one companion closer than 2.5 arcsec; 13 (23.2%) have at least one source within 3 arcsec; and another 13 KOIs (23.2%) present at least one object between 3−6 arcsec. These results are summarized in the last section of Table 6. Compared to the real KOIs sample, we can see that these values are similar. Indeed, we found the same rate of isolated targets in both samples. However, there is a slightly higher amount of close companions in this sample compared to the real KOIs.

Although the detected planets around these KOIs were rejected, the light curves of those presenting close sources should be re-analyzed by taking this into account. Depending on the causes that led the different works to demote these objects as candidates, some of them could change the properties of the transiting objects and, perhaps, return them back to the planet candidate status.

5. Comparison to other high spatial resolution techniques in the *Kepler* sample

There are three main techniques that provide high-resolution (diffraction limited) images from the ground: speckle imaging, adaptive optics, and lucky imaging. Regarding the high spatial resolution studies performed for the *Kepler* candidates, there are three main works that have provided exhaustive observations of the candidates appart from our survey. Howell et al. (2011, hereafter H11) published the first results of the speckle imaging observations for 156 KOIs, using the 3.5 m-telescope WIYN on Kitt Peak. Adams et al. (2012 , hereafter A12) and Adams et al. (2013) provided the adaptive optics multiplicity results in the near-infrared regime for a total of 102 KOIs using both the 6.5 m Multiple Mirror Telescope (MMT) and the Palomar Hale 5.1 m telescope. A posterior, shallow survey by Law et al. (2013) with Robo-AO (hereafter L13) provided adaptive optics observations for 715 *Kepler* candidates, using the robotic Palomar 1.5 m telescope (Cenko et al. 2006). The results of the current paper added to those of Lillo-Box et al. (2012) complete the set of high spatial resolution techniques by providing lucky imaging for 234 KOIs in the optical range.

The distribution of *Kepler* magnitudes is similar for all surveys, peaking L13 and the present work at slightly fainter

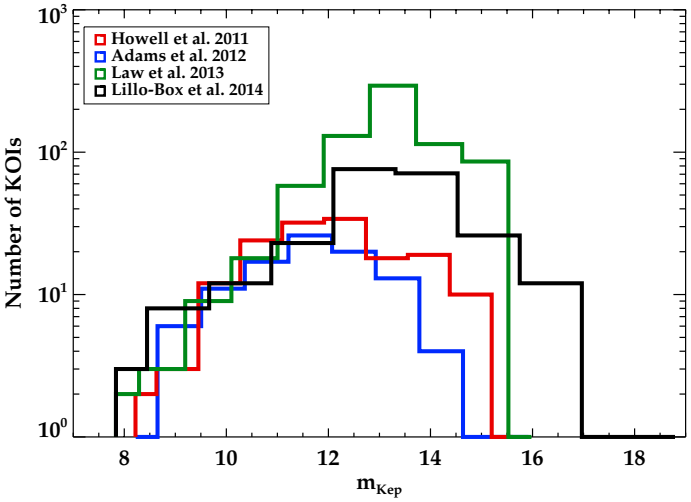

Fig. 8. Distributions of *Kepler* magnitudes for the different high-spatial resolution surveys in the *Kepler* sample of planet host candidates.

magnitudes ($m_{\rm kep} \approx 14$) than H11 and A12 ($m_{\rm kep} \approx 12$). In Fig. 8, we show this distribution for the four studies.

However, since these works were published, some of their KOIs have been rejected as planet candidates due to several reasons. In particular, 24 KOIs from H11 (out of 156, 15%), 16 KOIs from A12 (out of 102, 16%), and 17 KOIs from L13 (out of 714, 2.3%) currently do not present any planet candidate. In our case, the percentage of non-planet KOIs is slightly higher (56 out of 230, 24%) because we observed several KOIs, which still had the *non-dispositioned* flag in the *Kepler* archive (meaning that they did not yet passed all requirements to be planet candidates), in 2013 observing season.

The speckle imaging study by H11 provides the highest resolution images (with detection limits at 0.05 arcsec) but in a very small field of view that only allows to detect companions at a limiting separation of 1.4 arcsec. They also provide a typical depth magnitude limitation of $\Delta m = 4.0$ mag. The large majority of the transits of planet candidates could be mimicked by blended stellar systems fainter than this magnitude difference (as we can see in the fourth column of Table 7). With these observing limitations, they found that four out of the 127 KOIs (3%) with remaining planet candidates do present a stellar companion closer than 1.4 arcsec.

The adaptive optics work by A12 seems to be more complete in magnitude depth and field coverage (more than 20 × 20 arcsec). We have used their updated Tables 2 and 4 to compute statistics that could be compared to the H11 and our own study. In particular, they find that among their 85 KOIs with remaining planet candidates, 37 are isolated (no companion closer than 6 arcsec, 44%), 12 KOIs (14%) present a stellar companion within 1.4 arcsec, 28 KOIs (33%) present a stellar companion within 3 arcsec, and 30 KOIs (35%) present at least one companion in the range 3–6 arcsec.

The recently published survey by Law et al. (2013) provides the largest catalog of AO observations of *Kepler* candidates. Their observations determine that 29 out of the 697 KOIs with remaining candidates (4.2%) present some companion within 1.4 arcsec, and 49 (7%) do present companions closer than 2.5 arcsec. Since this survey is limited to 2.5 arcsec of separation, we cannot include the remaining 648 in the isolated group.

All these numbers are summarized and compared to the lucky imaging results provided in this paper in Tables 6 and 9. Figure 9 also illustrates the coincident KOIs between the different surveys. In the next subsections, we compare these works to our survey summarizing coincident objects and BSC results. For the latter, please note that all four studies provide 5σ level sensitivity limits, so that direct comparisson of the BSC values can be done.

Table 9. Summary of coincident KOIs in the main high-resolution surveys of the *Kepler* sample.

	Lillo-Box	Adams+12	Howell+11	Law+13
Lillo-Box	230	10	12	112
Adams+12		102	74	66
Howell+11			156	85
Law+13				714

5.1. Comparison with Howell et al. (2011)

Among the 12 coincident objects between H11 and this work, none do present companions within 1.4 arcsec (the largest separation detectable by H11). Since sensitivity curves and photometric transformations of the filters used to the SDSS system are not provided by the authors for these targets, we cannot exactly compare how both studies have improved the BSC values. As a zero-order approximation, we can assume that the limiting magnitude presented in their Table 2 as $\Delta_{\rm max}$ and calculated for an angular separation of 0.2 arcsec is constant over the 1.4 arcsec of spatial coverage and obtained in a similar filter[10]. We can then determine a zero-order $\rm BSC_{H11}$ and thus compare to our values. The results (see Table 10) show that the speckle-imaging limiting magnitudes are smaller than the required magnitude differences for discarding possible background configurations that are able to mimic the planetary transit (that we have called $\Delta m_{\rm max}$ in this paper). This happens for all 32 planet candidates orbiting the 12 common KOIs. In all cases, our AstraLux observations are better (in terms of reducing the BSC parameter) than the H11 observations. The small contribution of the H11 study to reduce the probability of a blended eclipsing binary is mostly due to the reduced field of view, which avoids detection of 1.5−3.0 arcsec companions, where the probability of having a background source is maximum in the 0–3 arcsec range.

5.2. Comparison with Adams et al. (2012)

Only four out of the ten coincident objects with Adams et al. (2012) do present at least one companion below 6 arcsec.

KOI-0111 & KOI-0555. The companions to KOI-0111 and KOI-0555 detected by this work are not detected by A12. Since the magnitude differences in both cases are relatively small ($\Delta_i = 6.1$ for KOI-0111 and $\Delta_i = 3.8$ for KOI-0555), the non-detection by A12 could mean that these companions are bluer, but we would need photometry in different bands to provide conclusions about this result.

KOI-0372. On the contrary, we do not detect any of the faint companions to KOI-0372 with $\Delta m_{\rm Kep} > 10.0$ due to their faintness. However, the maximum magnitude difference for a companion star that could mimic the planetary transit of the candidate KOI-0372.01 is $\Delta m_{\rm max} = 4.99$, so that the detected companions by A12 do not affect the planetary candidacy of this object.

[10] The filters used by H11 are similar to the *I* and *R* Johnson bands.

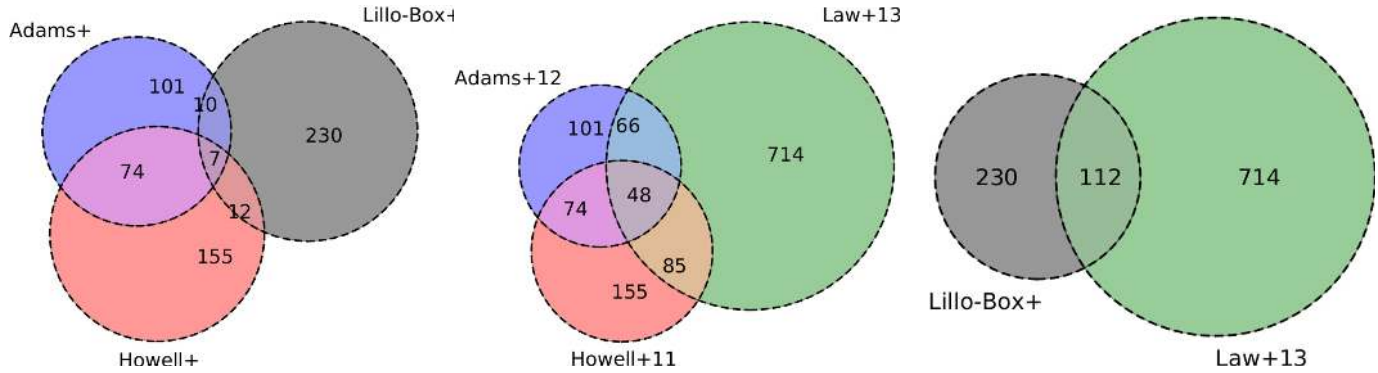

Fig. 9. Venn diagrams summarizing the results of the four main high spatial resolution studies regarding the *Kepler* sample of planet host candidates.

Table 10. Comparison between the improvements in the BSC parameter (in %) obtained by using the H11 (Howell et al. 2011), the A12 (Adams et al. 2012), and our high-resolution images (LB14) for all planet candidates involved (28 in H11 and 27 in A12).

Planet	$P_{BS,0}$	P_{BS} (%)			Planet	$P_{BS,0}$	P_{BS} (%)		
candidate	%	H11	A12	LB14	candidate	%	H11	A12	LB14
41.01	6.10	5.9	4.3	1.9 111.04	13.00	12.6	8.0	9.9	
41.02	10.10	9.9	8.2	5.8	115.01	4.50	–	2.5	1.9
41.03	9.40	9.2	7.6	5.2	115.02	7.40	–	5.4	4.8
49.01	8.10	7.4	–	3.4	115.03	14.80	–	12.8	12.2
69.01	4.10	4.0	2.0	1.5	196.01	4.00	2.8	–	0.4
82.01	1.30	1.2	0.4	0.2	245.01	0.90	0.9	0.3	0.1
82.02	2.50	2.4	1.5	1.0	245.02	2.30	2.3	1.7	1.3
82.03	3.10	3.0	2.1	1.6	245.03	5.30	5.3	4.7	4.2
82.04	4.20	4.1	3.2	2.7	245.04	4.10	4.1	3.5	3.1
82.05	5.30	5.2	4.3	3.8	366.01	2.40	2.0	–	0.7
94.01	3.70	3.1	0.9	0.3	372.01	4.20	3.4	0.2	0.8
94.02	10.60	10.0	6.5	4.1	398.01	3.80	2.5	–	0.9
94.03	6.80	6.2	2.7	1.2	398.02	8.50	7.2	–	5.4
94.04	23.80	23.2	19.7	17.2	398.03	13.50	12.2	–	10.4
111.01	5.40	5.1	0.9	2.3	638.01	15.20	–	3.2	8.8
111.02	5.60	5.3	1.0	2.6	638.02	14.60	–	2.7	8.3
111.03	4.90	4.6	0.7	1.9					

Notes. In all cases, the BSC has been improved with respect to the speckle images and the A12 study. Note that the common target KOI-0623 to H11 is not presented here because we detected a stellar companion closer than 3 arcsec. The small improvement of the H11 study is mostly due to the reduced field of view, which avoids detection of 1.5–3.0 arcsec companions, where the probability of having a background source is maximum in the 0–3 arcsec range.

KOI-0115. The latter case affects KOI-0115 with three planet candidates for which $\Delta m_{max}(.01) = 7.6$, $\Delta m_{max}(.02) = 8.8$, and $\Delta m_{max}(.03) = 11.1$. The observations from A12 detected two companions with magnitude differences below those values. We do not detect the closest target at 2.43 arcsec and $\Delta m_{kep} = 11.4$ mag due to sensitivity restrictions in the present study. However, this companion has a magnitude difference that is higher than the maximum difference that would affect any of the three planets detected in this system. Hence, we could say that this is a negligible blended star for this system.

In the case of the six remaining KOIs with non-detected companions closer than 6 arcsec, we obtain smaller values of the blended source probability, given that our images are deeper for these particular objects. Table 10 summarizes these results compared to our values according to the updated sensitivity limits that are provided by A12 for each target in the *Kepler* band and transformed to the i_{SDSS} filter using our own transformation determined in Sect. 4.1.1. In this case, we can see that A12 reduces the probability of having a background source more than H11. The only handicap of this survey is that possible blue non-negligible objects could not be detected by this survey (as we have shown in the cases of KOI-0555 or KOI-0111), since *Kepler* observations are performed in the optical wavelengths and A12 observations are obtained in *J* and *K*s bands.

5.3. Comparison with Law et al. (2013)

A total of 112 KOIs have counterparts in both L13 and the present study. Among this subsample, 13 KOIs have been detected to have companions within 2.5 arcsec (the largest separation that L13 can achieve). In four cases, both studies detect the companions (KOI-0401, KOI-0191, KOI-0628, and KOI-1375). In one case (KOI-0640), our survey does not detect the companion object at 0.44 arcsec with a contrast magnitude of 0.62 mag in the *i* band. We have examined the AstraLux image and concluded that the ambient conditions were poor for this particular night. This is also reflected in its sensitivity curve with poor quality. Finally, we have detected companions to the remaining eight KOIs (namely, KOI-0658, KOI-1452, KOI-0703, KOI-0704, KOI-0721, KOI-2481, KOI-0111, and KOI-1812) that

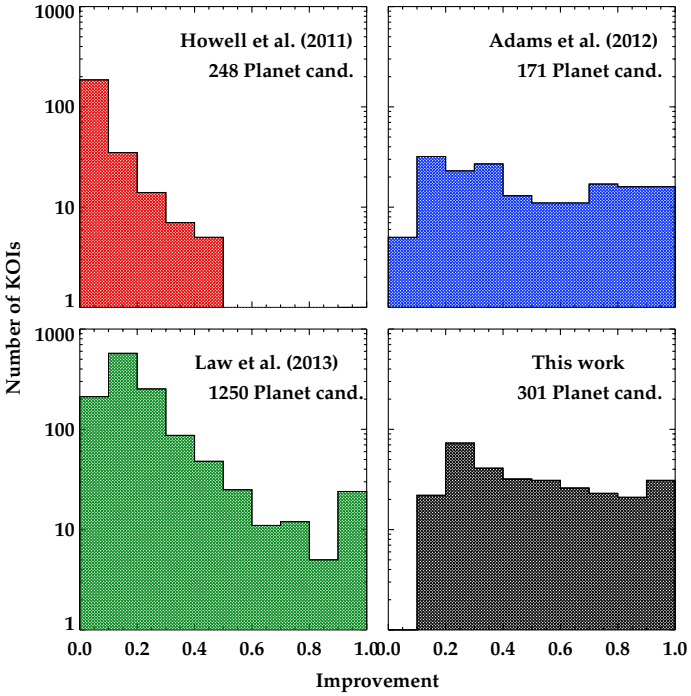

Fig. 10. Comparison of the quality of the four main high-resolution surveys of the *Kepler* sample of planet candidates. The *x*-axis represents the improvement in the probability of a background, non-detected companion that could mimic the particular planetary transit.

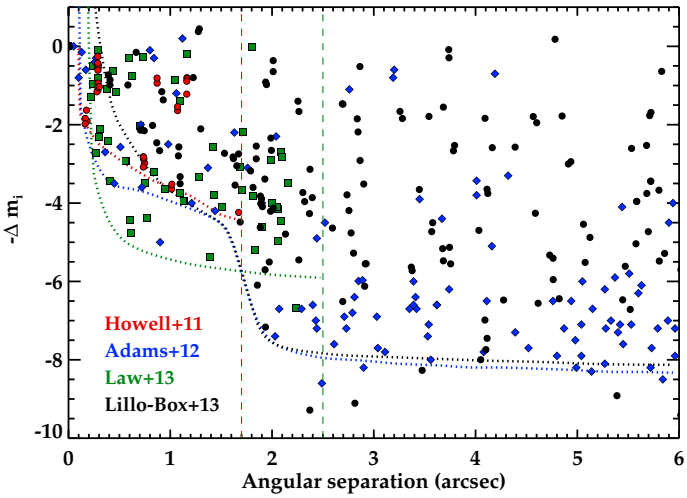

Fig. 11. All companions detected by the different high-resolution surveys studied in this work: Adams et al. (2012) in blue filled diamonds, Howell et al. (2011) in red filled circles, Law et al. (2013) in green filled squares, and our work in black filled circles. The empirical sensitivity limits according to these detections are shown with dotted lines.

were not detected by the L13 survey. In L13, the authors justify this non-detection compared to our previous study by arguing that the companions are fainter than their detections limits. However, all planet candidates in these eight planetary systems have calculated a $\Delta m_{\max}$ that is fainter than the calculated magnitude differences of the companion sources. Thus, the detected companions in our survey and those not detected by L13 can actually severely affect the candidacy of the planet candidates or, at least, their planet properties, which are, thus, non-negligible detections. It must be noted that we have detected companions in the range 2.5–6.0 arcsec for another 26 coincident KOIs that could also affect the derived properties of the planet candidate or even their candidacy and that they are not detected in L13 due to field of view restrictions.

Since no individual sensitivity limits are provided for each KOI in L13, we can use their quality definition for each KOI (low, medium, or high), use the correspondent sensitivity curve in the $i_{\rm SDSS}$ band provided in their paper to estimate the BSC, and compare it to the values found for our isolated KOIs. The results are presented and compared in Table 11. In general, our observations reduce the $P_{\rm BS}$ by a more significant amount.

5.4. General comparison of Kepler high-resolution imaging surveys

We can compare the results of the surveys by using the BSC parameter defined in previous sections. In particular, we can estimate how each of these high-resolution surveys have contributed to the validation of the planet candidates by measuring how it has diminished the probability of a KOI to have a blended non-detected source. We can calculate the BSC parameter for each observed target in each survey and compare the BSC value prior and after the imaging observations (as we have done in Sect. 4.1.1 for the KOIs observed in the present study). We can define the *Improvement* parameter as the relative difference between the prior BSC value and the new BSC value obtained with the high-resolution image (i.e. Improvement = $(P_{\rm BS,0} - P_{\rm BS})/P_{\rm BS,0}$). By doing so, we can summarize the results by the histogram shown in Fig. 10. According to this, we can see that A12 obtained a similar distribution of improvements than our work. The only handicap of this survey lies is that the targets were observed in the near-infrared while *Kepler* observations are performed in the optical band. Thus, they could miss some bluer companions that affect the *Kepler* photometry. This was demonstrated in Sect. 5.2 with the cases of KOI-0111 and KOI-0555. On the contrary, we could be missing redder companions that are possibly bound (such KOI-0372B), which could have implications in the knowledge of the formation and evolution of the planetary system.

The H11 speckle imaging study does not reduce the probability of a blended scenario in more than 10% for the large majority of their observations. This is mostly due to the limited contrast magnitude and small field of view that they use.

In the case of L13, they present the largest sample of high-resolution images, which are also observed in the optical range. Their distribution of improvement for L13 is rather broad. With these observations, the 93% of the planet candidates hosted by their observed KOIs (1163 planet candidates in total) diminish the probability of a blended scenario by less than 50%. The remaining 7% of the planet candidates (87 in total) reduced this probability by more than 50%. However, since we calculated their $P_{\rm BS}$ by assuming the typical sensitivity curves that are provided by L13 for each target, according to their quality definition of the AO image (namely *low*, *medium*, and *high*), we warn that applying the particular sensitivity curves for each KOI could significantly modify these results.

Finally, our survey provides high-resolution observations for 230 *Kepler* host candidates (174 still active KOIs) in the optical range. Our results show improvements in the blended source probability above 50% for the 62% of the planet candidates studied (186 in total) and below 50% for the remaining 38% of the planet candidates (115 in total).

In Fig. 11, we show all the companions detected by the four surveys. Empirical sensitivity curves according to these detections are also plotted for each of the surveys.

6. Conclusions

In this work, we have delivered a second release of high-resolution observations of *Kepler* candidates with the AstraLux/CAHA instrument. In total, 230 KOIs were observed, and 174 currently kept at least one of their planets as candidates. Our complete multiplicity study shows that 111 KOIs (67.2%) do not present any visual companion closer than 6 arcsec; 35 KOIs (20.1%) do present at least one source between 3–6 arcsec; and 30 KOIs (17.2%) present close companions within 3 arcsec. Among the new sample of close companions, we have concluded that KOI-3158B could be physically associated to the planet host, thus being an S-type binary system with multiple planet candidates orbiting one of the components of the binary. These results clearly shows the need for obtaining high-resolution images of planet candidates prior to starting the confirmation process by other (more expensive and time-consuming) techniques, such as radial velocity.

We have analyzed the quality of the images by defining the BSC parameter (background source confidence) that provides the level of confidence by which one can assure that the KOI is isolated within some specific magnitude difference and angular separation. We calculated the BSC parameter for all targets without close companions below 3 arcsec, reducing this probability by more than 50% for the 62% of our targets. This implies that thanks to the AstraLux observations we have increased the level of confidence that the KOIs are not blended by an eclipsing binary or affected by additional sources contaminating the *Kepler* light curve.

We have performed a comparison to the other three main catalogs of high-resolution images published so far. With the adaptive optics study by Adams et al. (2012, 2013) our conclusions show that our work reduces the blended source probability by a high percentage for the majority of the observed targets. The only handicap of the former study is that it is performed in the near-infrared regime; thus, it misses possible hotter companions that could affect the *Kepler* photometry obtained in the optical range. This becomes clear in the cases of KOI-0111 and KOI-0555, where we detect close companions non-detected by them. By contrast, we could be missing redder physically bound companions (although they do not affect the planet candidacy since the optical *Kepler* light curve would not be significantly affected). The other adaptive optics survey provides a large set of observations performed by a robotic telescope (Robo-AO) by Law et al. (2013). They obtained high-resolution images for 714 KOIs in the optical regime. However, although their resolution is high enough, their field of view is too limited (only detecting sources at less than 2.5 arcsec) and their limiting contrast is too small to improve the isolated confidence by more than 50% for a significant percentage of their candidates. Hence, this survey must be combined with other observations to achieve useful conclusions. Finally, the speckle study by Howell et al. (2011) is too limited in both field coverage and magnitude difference, although they achieve very high angular resolutions. This implies that they do not improve the isolation confidence for their targets by more than 10% and is, thus, not conclusive for this purpose.

In this paper, we have also included the high-spatial resolution results for the Kepler-186 (KOI-0571) system, hosting the recently validated planet Kepler-186f, an Earth-like planet in the habitable zone of its cool dwarf (Quintana et al. 2014). The authors obtained high-contrast images in the *K*s band using AO with NIRC2 at the Keck-II telescope and optical speckle imaging with DSSI at WIYN telescope. The present work adds additional observational support to the conclusion that Kepler-186 is isolated with optical information that is farther than the 1.2 arcsec of the WIYN observations and in the wavelength regime of *Kepler* observations.

Our high-resolution survey of *Kepler* candidates with similar important surveys has proven the need for complementary observations of the *Kepler* candidates.

Acknowledgements. This research has been funded by Spanish grants AYA 2010-21161-C02-02, AYA2012-38897-C02-01, and PRICIT-S2009/ESP-1496. J. Lillo-Box thanks the CSIC JAE-predoc programme for the Ph.D. fellowship. We also thank Calar Alto Observatory, both the open TAC and Spanish GTO panel, for allocating our observing runs, and the CAHA staff for their effort and passion in their work, being very helpful during our visitor and service AstraLux observations. This publication made use of VOSA, developed under the Spanish Virtual Observatory project supported from the Spanish MICINN through grant AyA2008-02156. We also thank the *Kepler* Team for providing valuable information about the targets to be observed. This paper made use of iPython (Pérez & Granger 2007), and the python libraries *numpy*, *matplotlib*, *matplotlib_venn*, and *asciitable*.

References

Adams, E. R., Ciardi, D. R., Dupree, A. K., et al. 2012, AJ, 144, 42
Adams, E. R., Dupree, A. K., Kulesa, C., & McCarthy, D. 2013, AJ, 146, 9
Barclay, T., Rowe, J. F., Lissauer, J. J., et al. 2013, Nature, 494, 452
Barrado, D., Lillo-Box, J., Bouy, H., Aceituno, J., & Sánchez, S. 2013, in EPJ Web Conf., 47, 5008
Batalha, N. M., Borucki, W. J., Koch, D. G., et al. 2010, ApJ, 713, L109
Batalha, N. M., Rowe, J. F., Bryson, S. T., et al. 2013, ApJS, 204, 24
Bayo, A., Rodrigo, C., Barrado Y Navascués, D., et al. 2008, A&A, 492, 277
Bayo, A., Rodrigo, C., Barrado, D., et al. 2013 [arXiv:1312.2739]
Borucki, W. J., Koch, D. G., Basri, G., et al. 2011, ApJ, 736, 19
Bouy, H., Bertin, E., Moraux, E., et al. 2013, A&A, 554, A101
Brown, T. M., Latham, D. W., Everett, M. E., & Esquerdo, G. A. 2011, AJ, 142, 112
Burke, C. J., Bryson, S., Christiansen, J., et al. 2013, in AAS Meeting Abstracts, 221, 216.02
Cabrera, J., Csizmadia, S., Lehmann, H., et al. 2014, ApJ, 781, 18
Cenko, S. B., Fox, D. B., Moon, D.-S., et al. 2006, PASP, 118, 1396
Chabrier, G. 2001, ApJ, 554, 1274
Chabrier, G., & Baraffe, I. 2000, ARA&A, 38, 337
Daemgen, S., Hormuth, F., Brandner, W., et al. 2009, A&A, 498, 567
Hormuth, F. 2007, AstraLux diploma thesis (University of Heidelberg)
Howell, S. B., Everett, M. E., Sherry, W., Horch, E., & Ciardi, D. R. 2011, AJ, 142, 19
Kley, W. 2010, in EAS Pub. Ser. 42, eds. K. Gożdziewski, A. Niedzielski, & J. Schneider, 227
Law, N. M., Morton, T., Baranec, C., et al. 2013 [arXiv:1312.4958]
Lillo-Box, J., Barrado, D., & Bouy, H. 2012, A&A, 546, A10
Lillo-Box, J., Barrado, D., Moya, A., et al. 2014, A&A, 562, A109
Lissauer, J. J., Marcy, G. W., Bryson, S. T., et al. 2014, ApJ, 784, 44
Marcy, G. W., Isaacson, H., Howard, A. W., et al. 2014, ApJS, 210, 20
Moraux, E., Bouvier, J., Stauffer, J. R., & Cuillandre, J.-C. 2003, A&A, 400, 891
Morton, T. D., & Johnson, J. A. 2011, ApJ, 738, 170
Ofek, E. O. 2008, PASP, 120, 1128
Pérez, F., & Granger, B. E. 2007, Comput. Sci. Eng., 9, 21
Pinsonneault, M. H., An, D., Molenda-Żakowicz, J., et al. 2012, ApJS, 199, 30
Quintana, E. V., Rowe, J. F., Barclay, T., et al. 2013, ApJ, 767, 137
Quintana, E. V., Barclay, T., Raymond, S. N., et al. 2014, Science, 344, 277
Rowe, J. F., Bryson, S. T., Marcy, G. W., et al. 2014, ApJ, 784, 45
Steffen, J. H., Ford, E. B., Rowe, J. F., et al. 2012, ApJ, 756, 186
Strehl, K. 1902, Astron. Nachr., 158, 89
Weiss, L. M., Marcy, G. W., Rowe, J. F., et al. 2013, ApJ, 768, 14
Yanny, B., Guhathakurta, P., Bahcall, J. N., & Schneider, D. P. 1994, AJ, 107, 1745

Pages 16 to 32 are available in the electronic edition of the journal at http://www.aanda.org

Table 1. Observational information, completeness, and detectability magnitudes for the isolated KOIs observed with the Calar Alto/AstraLux instrument during the 2011 observational season (62 KOIs in total) and all targets observed during 2012 and 2013 seassons (20 and 57 KOIs, respectively).

KOI ID	Others[a]	KIC	RA[b] J2000.0	Dec[b] J2000.0	kep mag	Date yyyy-mm-dd	Filter	T_{ind} s	#Frames	Eff.Time s	i_{comp}[c] mag	i_{det}[d] mag
Active KOIs												
12	L	5812701	19:49:48.9	41:00:39.56	11.353	2011-06-03	*i*	0.05	10000	50.0	16.9	20.2
41	H, A, L	6521045	19:25:32.64	41:59:24.97	11.197	2013-06-22	*i*	0.083	40000	332.0	19.0	22.3
49	H, L	9527334	19:28:59.77	46:09:53.36	13.704	2013-06-22	*i*	0.083	40000	332.0	19.0	22.3
51	–	6056992	19:43:40.52	41:19:56.76	13.761	2013-06-22	*i*	0.06	20000	120.0	17.8	21.1
69	H, A, L	3544595	19:25:40.39	38:40:20.49	9.931	2013-06-22	*i*	0.045	40000	180.0	18.3	22.6
82	H, A, L	10187017	18:45:55.85	47:12:28.91	11.492	2013-06-23	*i*	0.068	40000	272.0	18.7	22.0
94	H, A, L	6462863	19:49:19.94	41:53:28.04	12.205	2013-06-21	*i*	0.06	30000	180.0	18.3	21.6
111	H, A, L	6678383	19:10:25.11	42:10:00.4	12.596	2013-06-23	*i*	0.068	40000	272.0	18.7	22.0
115	A, L	9579641	19:11:32.96	46:16:34.47	12.791	2013-06-23	*i*	0.068	40000	272.0	18.7	22.0
139	L	8559644	19:26:36.76	44:41:17.78	13.492	2011-06-10	*i*	0.075	20000	150.0	18.1	21.4
149	L	3835670	19:06:31.22	38:56:44.16	13.397	2013-06-23	*i*	0.068	40000	272.0	18.7	22.0
152	L	8394721	20:02:04.11	44:22:53.69	13.914	2013-06-14	*i*	0.08	30000	240.0	18.6	21.9
156	L	10925104	19:36:29.14	48:20:58.28	13.738	2013-06-16	*i*	0.068	40000	272.0	18.7	22.0
191	L	5972334	19:41:08.94	41:13:19.05	14.991	2013-06-15	*i*	0.08	25000	200.0	18.4	21.7
191	L					2013-06-15	*z*	0.08	25000	200.0	–	–
196	H	9410930	19:38:03.18	45:58:53.9	14.465	2011-05-10	*i*	0.2	10000	200.0	18.4	21.7
199	–	10019708	19:40:06.16	46:57:21.6	14.879	2011-05-12	*i*	0.2	10000	200.0	18.4	21.7
209	L	10723750	19:15:10.33	48:02:24.83	14.274	2011-06-06	*i*	0.1	20000	200.0	18.4	21.7
211	L	10656508	19:11:52.87	47:58:19.56	14.989	2011-06-08	*i*	0.1	30000	300.0	18.8	22.1
238	L	7219825	19:47:59.67	42:46:55.06	14.061	2011-06-05	*i*	0.1	20000	200.0	18.4	21.7
245	H, A	8478994	18:56:14.29	44:31:05.57	9.705	2012-05-27	*i*	0.03	30000	90.0	17.5	20.8
330	L	11361646	19:47:26.21	49:09:43.37	13.928	2011-06-26	*i*	0.1	20000	200.0	18.4	21.7
338	–	10552611	19:51:53.01	47:43:54.06	13.448	2011-06-01	*i*	0.087	10000	87.0	17.5	20.8
338	–					2011-06-01	*z*	0.09	10000	90.0	–	–
339	L	10587105	19:03:33.21	47:52:49.36	13.763	2011-06-26	*i*	0.1	20000	200.0	18.4	21.7
345	L	11074541	19:06:05.95	48:41:00.96	13.34	2011-06-03	*i*	0.09	10000	90.0	17.5	20.8
346	–	11100383	19:54:38.62	48:36:22.93	13.524	2011-06-04	*z*	0.15	12000	180.0	–	–
349	L	11394027	19:07:24.64	49:15:42.05	13.586	2011-06-04	*i*	0.15	12000	180.0	18.3	21.6
351	–	11442793	18:57:44.04	49:18:18.58	13.804	2011-06-03	*i*	0.2	12000	240.0	18.6	21.9
366	H, L	3545478	19:26:39.4	38:37:09.32	11.714	2011-06-01	*i*	0.034	10000	34.0	16.5	19.8
372	H, A, L	6471021	19:56:29.38	41:52:00.34	12.391	2011-06-01	*i*	0.034	10000	34.0	16.5	19.8
372	H, A, L					2011-06-01	*z*	0.04	10000	40.0	–	–
385	L	3446746	19:28:51.62	38:32:54.93	13.435	2011-06-03	*i*	0.2	10000	200.0	18.4	21.7
386	L	3656121	19:36:26.58	38:42:36.84	13.838	2011-05-10	*i*	0.2	10000	200.0	18.4	21.7
388	L	3831053	18:58:49.66	38:56:12.56	13.644	2011-06-04	*i*	0.15	12000	180.0	18.3	21.6
393	L	3964109	19:36:06.99	39:03:06.66	13.542	2011-06-05	*i*	0.15	10000	150.0	18.1	21.4
398	H	9946525	19:19:08.69	46:51:31.65	15.342	2013-06-22	*i*	0.09	29999	270.0	18.7	22.0
416	L	6508221	19:07:27.71	41:59:20.68	14.29	2011-06-06	*i*	0.1	20000	200.0	18.4	21.7
422	–	9214713	19:21:33.56	45:39:55.18	14.74	2011-06-25	*i*	0.2	10000	200.0	18.4	21.7
422	–					2011-06-25	*z*	0.1	20000	200.0	–	–
431	L	10843590	18:49:50.52	48:15:25.62	14.262	2011-06-07	*i*	0.1	20000	200.0	18.4	21.7
435	L	11709124	19:19:07.32	49:53:47.51	14.534	2013-06-14	*i*	0.08	30000	240.0	18.6	21.9
463	L	8845205	20:00:49.46	45:01:05.3	14.708	2011-06-25	*i*	0.1	20000	200.0	18.4	21.7
473	–	10155434	19:47:14.08	47:10:18.98	14.673	2011-06-08	*i*	0.1	20000	200.0	18.4	21.7
478	L	10990886	19:52:25.37	48:24:04.14	14.273	2011-06-01	*i*	0.15	10000	150.0	18.1	21.4
481	L	11192998	19:32:38.44	48:52:52.29	14.701	2011-06-09	*i*	0.1	20000	200.0	18.4	21.7
496	–	4454752	19:15:01.19	39:33:49.13	14.411	2011-06-01	*i*	0.2	10000	200.0	18.4	21.7
518	–	8017703	19:09:45.4	43:49:55.52	14.287	2013-06-22	*i*	0.083	40000	332.0	19.0	22.3
524	–	8934495	18:54:10.6	45:13:31.99	14.868	2011-06-09	*i*	0.1	23000	230.0	18.6	21.9
528	L	9941859	19:08:24.27	46:53:47.33	14.598	2011-06-08	*i*	0.1	20000	200.0	18.4	21.7
534	L	10554999	19:54:39.29	47:45:43.34	14.613	2011-05-10	*i*	0.2	10000	200.0	18.4	21.7
561	L	6665695	18:48:01.11	42:10:35.5	14.005	2011-05-10	*i*	0.2	8000	160.0	18.2	21.5
564	L	6786037	19:37:07.43	42:17:27.49	14.854	2013-06-15	*i*	0.08	33750	270.0	18.7	22.0
567	L	7445445	19:27:48.46	43:04:28.96	14.338	2011-06-01	*i*	0.2	10000	200.0	18.4	21.7
571	L	8120608	19:54:36.65	43:57:18.08	14.625	2011-06-08	*i*	0.1	20000	200.0	18.4	21.7

Notes. The targets with close companions from 2011 (another 41 KOIs) were already published in Lillo-Box et al. (2012). Active KOIs (currently keeping at least one of their planet candidates) are shown in the upper part of the table and demoted KOIs are shown in the bottom part of the table. [(a)] Identifier of papers where high-resolution images are provided for each KOI: H for Howell et al. (2011), A for Adams et al. (2012), and L for Law et al. (2013). [(b)] Right ascension and declination from Borucki et al. (2011). [(c)] Estimated completeness magnitudes scaled to those found for the 200 s image of the globular cluster M15. [(d)] Estimated detectability magnitudes scaled to those found for the 200 s image of the globular cluster M15.

Table 1. continued.

KOI ID	Others[a]	KIC	RA[b] J2000.0	Dec[b] J2000.0	kep mag	Date yyyy-mm-dd	Filter	T_{ind} s	#Frames	Eff.Time s	i_{comp}[c] mag	i_{det}[d] mag
579	L	8616637	19:14:20.17	44:44:01.68	14.137	2011-06-05	*i*	0.1	20000	200.0	18.4	21.7
611	L	6309763	19:53:10.57	41:41:01.68	14.022	2011-06-02	*i*	0.2	10000	200.0	18.4	21.7
617	–	9846086	19:49:40.48	46:38:39.34	14.608	2011-06-06	*i*	0.1	20000	200.0	18.4	21.7
624	L	3541946	19:22:41.55	38:41:27.64	13.597	2013-06-15	*i*	0.083	40000	332.0	19.0	22.3
625	L	4449034	19:06:15.31	39:32:04.09	13.592	2011-06-10	*i*	0.075	20000	150.0	18.1	21.4
632	L	4827723	19:17:40.28	39:56:42.04	13.359	2011-05-12	*i*	0.15	10000	150.0	18.1	21.4
638	A, L	5113822	19:42:14.26	40:14:10.58	13.595	2011-06-05	*i*	0.1	14000	140.0	18.0	21.4
640	L	5121511	19:49:00.63	40:17:18.96	13.332	2013-06-21	*i*	0.083	40000	332.0	19.0	22.3
650	L	5786676	19:21:35.08	41:02:24.29	13.594	2013-06-21	*i*	0.083	7766	64.5	17.2	20.5
654	L	5941160	18:57:38.38	41:14:14.86	13.984	2011-06-10	*i*	0.075	20000	150.0	18.1	21.4
659	L	6125481	19:29:40.13	41:25:00.73	13.413	2011-05-12	*i*	0.15	14000	210.0	18.5	21.8
664	L	6442340	19:26:32.32	41:50:01.89	13.484	2011-06-26	*i*	0.075	20000	150.0	18.1	21.4
670	–	7033671	19:27:17.64	42:30:58.35	13.774	2011-06-26	*i*	0.1	20000	200.0	18.4	21.7
672	–	7115785	19:24:40.69	42:38:26.91	13.998	2013-06-21	*i*	0.083	10498	87.1	17.5	20.9
676	L	7447200	19:30:00.81	43:04:59.34	13.822	2011-06-05	*i*	0.1	14000	140.0	18.0	21.2
678	–	7509886	19:01:45.4	43:10:06.53	13.283	2011-06-25	*i*	0.1	14000	140.0	18.0	21.3
682	L	7619236	19:40:47.52	43:16:10.23	13.916	2013-06-10	*i*	0.05	45000	225.0	18.5	21.8
684	L	7730747	18:45:09.67	43:24:48.03	13.831	2011-06-10	*i*	0.075	20000	150.0	18.1	21.4
686	L	7906882	19:47:21.78	43:38:49.64	13.579	2011-06-10	*i*	0.075	20000	150.0	18.1	21.4
693	–	8738735	18:59:01.16	44:57:21.72	13.949	2011-06-25	*i*	0.1	20000	200.0	18.4	21.7
695	L	8805348	19:02:37.43	45:04:46.41	13.437	2011-06-03	*i*	0.15	12000	180.0	18.3	21.6
709	L	9578686	19:09:19.87	46:12:12.64	13.94	2011-06-25	*i*	0.1	20000	200.0	18.4	21.7
717	L	9873254	18:48:51.1	46:43:04.15	13.387	2011-06-26	*i*	0.1	14000	140.0	18.0	21.3
739	L	10386984	18:51:56.11	47:34:42.92	15.488	2011-05-10	*i*	0.2	10000	200.0	18.4	21.7
800	L	3342970	19:26:36.85	38:29:40.77	15.541	2011-05-08	*i*	0.2	10000	200.0	18.4	21.7
800	L					2011-05-11	*z*	0.2	7580	151.6	–	–
834	L	5436502	19:11:35.31	40:38:16.16	15.084	2013-06-15	*i*	0.08	38000	304.0	18.9	22.2
884	L	7434875	19:14:34.2	43:02:21.45	15.067	2011-06-09	*i*	0.1	24000	240.0	18.6	21.9
1096	–	3230491	19:20:43.93	38:19:18.99	14.709	2013-06-10	*i*	0.09	30000	270.0	18.7	22.0
1174	–	10287723	19:47:17.19	47:21:14.51	13.447	2013-06-20	*i*	0.068	40000	272.0	18.7	22.0
1230	L	6470149	19:55:47.56	41:48:43.74	12.263	2013-06-12	*i*	0.04	40000	160.0	18.2	21.5
1236	L	6677841	19:09:33.89	42:11:41.4	13.659	2011-06-10	*i*	0.075	20000	150.0	18.1	21.4
1268	–	8813698	19:19:33.51	45:00:20.41	14.814	2011-06-07	*i*	0.15	20000	300.0	18.8	22.1
1353	L	7303287	19:49:51.68	42:52:58.22	13.956	2012-05-26	*i*	0.075	30000	225.0	18.5	21.6
1356	–	7363829	19:28:28.78	42:55:54.04	15.206	2013-06-11	*i*	0.1	30000	300.0	18.8	22.1
1421	–	11342550	19:10:36.11	49:09:21.79	15.305	2013-06-11	*i*	0.1	30000	300.0	18.8	22.1
1426	L	11122894	18:52:50.2	48:46:39.51	14.232	2011-06-25	*i*	0.1	20000	200.0	18.4	21.7
1452	L	7449844	19:33:07.57	43:03:20.91	13.63	2012-05-26	*i*	0.075	30000	225.0	18.5	21.8
1477	–	7811397	19:10:36.95	43:30:20.58	15.917	2013-06-11	*i*	0.1	30000	300.0	18.8	22.1
1529	L	9821454	19:08:09.48	46:38:24.46	14.307	2011-06-08	*i*	0.1	20000	200.0	18.4	21.7
1546	–	5475431	19:54:03.29	40:38:22.64	14.456	2013-07-16	*i*	0.08	22500	180.0	18.3	21.6
1596	L	10027323	19:50:02.37	46:57:40.54	15.157	2011-06-09	*i*	0.1	24000	240.0	18.6	21.9
1684	L	6048024	19:34:08.28	41:19:47.64	12.849	2012-05-25	*i*	0.075	30000	225.0	18.5	21.8
1701	L	7222086	19:50:04.58	42:46:37.42	11.041	2012-05-27	*i*	0.05	30000	150.0	18.1	21.4
1725	L	10905746	18:54:30.92	48:23:27.61	13.496	2013-06-13	*i*	0.04	40000	160.0	18.2	21.5
1779	L	9909735	19:53:55.88	46:47:37.04	13.297	2012-05-25	*i*	0.09	25000	225.0	18.5	21.8
1781	L	11551692	19:10:25.34	49:31:23.73	12.231	2012-05-25	*i*	0.05	30000	150.0	18.1	21.4
1800	–	11017901	19:01:04.46	48:33:36.03	12.394	2012-05-25	*i*	0.05	30000	150.0	18.1	21.4
1802	L	11298298	19:30:07.4	49:03:42.16	13.345	2013-06-16	*i*	0.083	40000	332.0	19.0	22.3
1805	L	4644952	19:15:14.87	39:46:14.38	13.828	2013-06-20	*i*	0.083	40000	332.0	19.0	22.3
1812	L	6279974	19:20:30.37	41:36:03.9	13.742	2013-06-19	*i*	0.068	40000	272.0	18.7	22.0
1894	L	11673802	19:49:26.23	49:47:51.18	13.427	2012-05-25	*i*	0.07	35000	245.0	18.6	21.9
1925	L	9955598	19:34:43.01	46:51:09.94	9.439	2012-05-27	*i*	0.03	30000	90.0	17.5	20.8
2042	L	9111849	19:55:00.04	45:27:59.04	13.089	2012-05-25	*i*	0.075	30000	225.0	18.5	21.8
2133	L	8219268	19:02:41.49	44:07:00.23	12.495	2012-05-25	*i*	0.05	30000	150.0	18.1	21.4
2260	L	11811193	19:20:56.6	50:01:48.32	12.168	2012-05-27	*i*	0.05	30000	150.0	18.1	21.4
2324	–	7746958	19:18:42.69	43:27:29.28	11.671	2012-05-27	*i*	0.05	30000	150.0	18.1	21.4
2352	L	8013439	19:00:43.87	43:49:51.88	10.421	2012-05-26	*i*	0.03	30000	90.0	17.5	20.8
2481	L	4476423	19:39:07.76	39:35:47.47	13.605	2012-05-26	*i*	0.05	30000	150.0	18.1	21.4
2481	L					2012-05-26	*z*	0.075	30000	225.0	–	–
2545	L	9696358	18:58:22.49	46:26:59.21	11.752	2012-05-26	*i*	0.03	30000	90.0	17.5	20.8
2593	L	8212002	18:47:20.48	44:09:21.3	11.714	2012-05-26	*i*	0.04	30000	120.0	17.8	21.1
2632	L	11337566	18:57:41.45	49:06:22.39	11.392	2012-05-26	*i*	0.05	30000	150.0	18.1	21.4
2640	L	9088780	19:27:14.36	45:26:07.72	13.226	2012-05-25	*i*	0.075	30000	225.0	18.5	21.8

Table 1. continued.

KOI ID	Others[a]	KIC	RA[b] J2000.0	Dec[b] J2000.0	kep mag	Date yyyy-mm-dd	Filter	T_{ind} s	#Frames	Eff.Time s	i_{comp}[c] mag	i_{det}[d] mag
2674	–	8022489	19:18:36.3	43:49:27.92	13.349	2013-06-14	*i*	0.08	30000	240.0	18.6	21.9
2712	–	11098013	19:50:59.35	48:41:39.51	11.125	2013-06-19	*i*	0.068	40000	272.0	18.7	22.0
3158	–	6278762	19:19:00.55	41:38:04.58	8.717	2013-06-15	*i*	0.03	40000	120.0	17.8	21.1
3158	–					2013-06-15	*z*	0.03	20000	60.0	–	–
3179	–	6153407	19:57:12.67	41:26:27.66	10.884	2013-06-19	*i*	0.083	40000	332.0	19.0	22.3
3203	–	3122872	19:31:34.12	38:16:13.84	11.816	2013-06-19	*i*	0.083	40000	332.0	19.0	22.3
3206	–	5612697	19:18:17.91	40:48:27.34	11.843	2013-06-19	*i*	0.083	40000	332.0	19.0	22.3
3237	–	6587796	19:01:19.35	42:02:25.54	12.325	2013-06-16	*i*	0.068	40000	272.0	18.7	22.0
3263	–	11853130	19:00:23.01	50:06:03.46	15.949	2013-06-11	*i*	0.07	43000	301.0	18.8	22.1
3444	–	5384713	19:49:43.01	40:33:42.87	13.693	2013-06-15	*i*	0.06	40000	240.0	18.6	21.9
3444	–					2013-06-15	*z*	0.06	30000	180.0	–	–
3554	–	6426592	19:02:24.39	41:49:03.12	15.207	2013-06-28	*i*	0.09	13333	120.0	17.8	21.1
3560	–	4848423	19:40:52.19	39:54:36.15	11.825	2013-07-14	*i*	0.04	30000	120.0	17.8	21.1
3649	–	6066379	19:52:31.79	41:20:03.37	15.475	2013-07-17	*i*	0.09	20000	180.0	18.3	21.6
3692	–	5903301	19:54:38	41:08:19.98	15.149	2013-07-17	*z*	0.09	29999	270.0	–	–
3728	–	7515679	19:11:13.73	43:11:19.62	12.252	2013-06-11	*i*	0.05	40000	200.0	18.4	21.7
3742	–	5565486	19:57:30.74	40:45:26.49	14.964	2013-06-29	*i*	0.09	13333	120.0	17.8	21.1
3765	–	12109845	19:23:40.6	50:41:47	16.44	2013-07-14	*i*	0.1	18000	180.0	18.3	22.4
3765	–					2013-07-17	*z*	0.1	18000	180.0	–	–
3801	–	8827930	19:40:49.67	45:05:53.48	15.999	2013-06-11	*i*	0.07	43000	301.0	18.8	22.1
3853	–	2697935	19:09:52.29	37:57:59.9	10.63	2013-06-28	*i*	0.045	40000	180.0	18.3	21.6
3886	–	8848288	20:04:11.35	45:05:15.47	9.837	2013-06-10	*i*	0.0295	25000	73.9	17.3	20.6
3886	–					2013-06-10	*z*	0.03	20000	60.0	–	–
3890	–	8564976	19:35:05.31	44:38:18.49	13.226	2013-06-13	*i*	0.05	35000	175.0	18.3	21.6
3925	–	10788461	19:12:39	48:09:54.54	14.026	2013-06-14	*i*	0.08	40000	320.0	18.9	22.2
4016	–	5938970	18:53:22.68	41:12:06.26	14.073	2013-06-16	*i*	0.083	36765	305.1	18.9	22.2
4351	–	5436161	19:11:02.2	40:39:25.34	14.999	2013-07-15	*i*	0.09	29999	270.0	18.7	22.0
4512	–	12069414	19:41:48.14	50:32:31.6	15.314	2013-07-16	*i*	0.09	36666	330.0	18.9	22.2
					Demoted KOIs							
6	–	3248033	19:38:23.89	38:22:00.38	12.161	2013-06-23	*i*	0.068	40000	272.0	18.7	22.0
1187	–	3848972	19:24:17.1	38:59:56.54	14.489	2013-06-20	*i*	0.083	40000	332.0	19.0	22.3
1924	L	5108214	19:37:08.86	40:12:49.72	7.837	2012-05-27	*i*	0.03	30000	90.0	17.5	20.8
3157	–	8738244	18:57:58.95	44:59:17.24	8.163	2013-07-16	*i*	0.045	40000	180.0	18.3	21.6
3178	–	10991239	19:52:56.44	48:29:52.4	10.863	2013-07-16	*i*	0.04	30000	120.0	17.8	21.1
3564	–	10960995	18:53:16.29	48:24:16.55	14.498	2013-07-14	*i*	0.08	15000	120.0	17.8	21.1
3570	–	5023948	19:40:57.83	40:09:27.36	15.048	2013-07-14	*i*	0.09	13333	120.0	17.8	21.1
3571	–	5113053	19:41:33.93	40:13:00.37	15.519	2013-07-14	*i*	0.09	13333	120.0	17.8	21.1
3588	–	9656543	19:39:04.47	46:22:27.16	16.319	2013-07-15	*i*	0.1	12000	120.0	17.8	21.1
3597	–	9366988	19:59:53.17	45:48:42.96	14.371	2013-07-15	*i*	0.08	15000	120.0	17.8	21.1
3616	–	6058875	19:45:28.89	41:23:25.69	15.839	2013-07-15	*i*	0.09	20000	180.0	18.3	21.6
3616	–	6058875	19:45:28.89	41:23:25.69	15.839	2013-07-17	*z*	0.09	20000	180.0	–	–
3633	–	11858741	19:15:02.47	50:10:36.6	16.485	2013-07-17	*z*	0.1	12000	120.0	–	–
3639	–	10491544	19:55:38.8	47:39:29.87	13.436	2013-06-10	*z*	0.05	30000	150.0	–	–
3639	–	10491544	19:55:38.8	47:39:29.87	13.436	2013-06-28	*i*	0.06	20000	120.0	17.8	21.1
3658	–	1575690	19:27:31.66	37:11:20.8	15.625	2013-07-15	*i*	0.09	20000	180.0	18.3	21.6
3670	–	2167890	19:32:22.47	37:30:52.24	12.858	2013-06-12	*z*	0.04	20000	80.0	–	–
3684	–	9394601	19:08:36.75	45:59:01.78	12.29	2013-07-15	*i*	0.06	20000	120.0	17.8	21.1
3684	–	9394601	19:08:36.75	45:59:01.78	12.29	2013-07-17	*z*	0.1	20000	200.0	–	–
3693	–	7695087	19:43:13.4	43:18:16.02	14.734	2013-06-12	*i*	0.07	35000	245.0	18.6	21.9
3704	–	2569494	19:20:42.92	37:50:56.22	17.38	2013-07-17	*i*	0.1	18000	180.0	18.3	21.6
3706	–	7770471	19:48:43.32	43:28:37.6	14.62	2013-07-15	*i*	0.08	15000	120.0	17.8	21.1
3708	–	6314173	19:56:57.75	41:37:18.05	17.719	2013-07-14	*i*	0.1	18000	180.0	18.3	21.6
3712	–	2437060	19:20:47.89	37:46:37.16	16.988	2013-06-12	*i*	0.1	20000	200.0	18.4	21.7
3714	–	11564013	19:37:16.59	49:31:55.67	15.207	2013-07-14	*i*	0.09	29999	270.0	18.7	22.0
3719	–	9837083	19:37:16.66	46:37:10.55	16.18	2013-07-15	*i*	0.1	18000	180.0	18.3	21.6
3719	–	9837083	19:37:16.66	46:37:10.55	16.18	2013-07-17	*i*	0.1	18000	180.0	18.3	21.6
3723	–	5471606	19:50:47.94	40:38:29.28	10.82	2013-07-14	*i*	0.04	30000	120.0	17.8	21.1
3725	–	3459199	19:40:48.69	38:31:10.38	10.055	2013-06-10	*i*	0.03	25000	75.0	17.3	20.6
3727	–	12023089	19:46:21.96	50:29:24.1	15.626	2013-07-13	*i*	0.09	36666	330.0	18.9	22.2
3730	–	10879213	19:53:02.38	48:13:08.27	18.792	2013-07-13	*i*	0.1	18000	180.0	18.3	21.6
3744	–	11303811	19:40:14.77	49:02:47.61	15.77	2013-07-13	*i*	0.09	36666	330.0	18.9	22.2
3763	–	3114667	19:23:59.34	38:16:57.42	17.375	2013-07-12	*i*	0.1	18000	180.0	18.3	21.6
3777	–	4075067	19:43:28.67	39:09:31.72	11.5	2013-06-13	*i*	0.04	40000	160.0	18.2	21.5

Table 1. continued.

KOI ID	Others[a]	KIC	RA[b] J2000.0	Dec[b] J2000.0	kep mag	Date yyyy-mm-dd	Filter	T_{ind} s	#Frames	Eff.Time s	i_{comp}[c] mag	i_{det}[d] mag
3788	–	9405541	19:29:45.43	45:57:08.49	9.687	2013-06-10	*i*	0.03	45000	135.0	18.0	21.3
3793	–	4037163	19:00:19.23	39:11:02.04	16.675	2013-06-29	*i*	0.1	27000	270.0	18.7	22.0
3795	–	3338660	19:21:53.81	38:25:38.52	14.807	2013-06-28	*i*	0.08	15000	120.0	17.8	21.1
3796	–	3338674	19:21:54.51	38:25:36.88	12.708	2013-06-11	*i*	0.05	40000	200.0	18.4	21.7
3800	–	9593759	19:36:25.76	46:12:34.09	17.474	2013-06-13	*i*	0.1	18090	180.9	18.3	21.6
3803	–	6286155	19:28:40.58	41:37:11.13	13.763	2013-06-12	*i*	0.07	40000	280.0	18.8	22.1
3805	–	4663185	19:36:19.05	39:43:46.71	11.356	2013-06-13	*i*	0.03	30000	90.0	17.5	20.8
3810	–	5769943	18:55:00.1	41:05:09.64	16.758	2013-06-29	*i*	0.1	27000	270.0	18.7	22.0
3814	–	2997178	19:32:17.95	38:10:10.99	12.861	2013-06-12	*i*	0.04	40000	160.0	18.2	21.5
3817	–	5636642	19:45:19.4	40:53:46.53	16.428	2013-06-29	*i*	0.1	33000	330.0	18.9	22.2
3821	–	5956776	19:22:35.59	41:14:02.65	16.747	2013-06-28	*i*	0.1	33000	330.0	18.9	22.2
3824	–	6516874	19:20:23.27	41:58:14.45	15.896	2013-06-28	*i*	0.09	36666	330.0	18.9	22.2
3827	–	5114623	19:42:55.88	40:15:38.81	15.36	2013-06-12	*i*	0.08	40000	320.0	18.9	22.2
3842	–	9532637	19:37:26.32	46:07:31.4	17.453	2013-07-13	*i*	0.1	18000	180.0	18.3	21.6
3845	–	11824218	19:46:27.82	50:01:18.15	13.724	2013-06-13	*i*	0.07	40000	280.0	18.8	22.1
3849	–	8949316	19:22:04.55	45:14:07.34	16.182	2013-07-13	*i*	0.1	27000	270.0	18.7	22.0
3873	–	8430105	19:26:14.07	44:29:17.48	10.42	2013-06-13	*i*	0.03	30000	90.0	17.5	20.8
3919	–	4649440	19:20:33.05	39:45:54.73	12.956	2013-06-13	*i*	0.07	35000	245.0	18.6	21.9
3940	–	5195945	19:37:15.09	40:19:11	12.93	2013-06-13	*i*	0.06	40000	240.0	18.6	21.9
3993	–	2970804	19:04:25.67	38:06:27.46	9.16	2013-06-29	*i*	0.03	40000	120.0	17.8	21.1
3998	–	7707742	19:55:35.89	43:23:44.31	16.975	2013-06-29	*i*	0.1	33000	330.0	18.9	22.2
4013	–	4832225	19:22:59.19	39:54:39.71	9.072	2013-07-16	*i*	0.068	40000	272.0	18.7	22.0
4013	–	4832225	19:22:59.19	39:54:39.71	9.072	2013-07-17	*z*	0.068	40000	272.0	–	–
4033	–	4138557	19:02:22.1	39:12:22.56	11.968	2013-07-16	*i*	0.06	30000	180.0	18.3	21.6
4033	–	4138557	19:02:22.1	39:12:22.56	11.968	2013-07-17	*z*	0.06	30000	180.0	–	–
4355	–	4571004	19:36:49.89	39:40:48.41	13.482	2013-06-28	*i*	0.083	40000	332.0	19.0	22.3

Table 3. Photometry of the 23 active KOIs (upper part of the table) and 18 demoted KOIs (bottom part of the table) with detected companions that are closer than 6 arcsec in the new sample observed during 2012 and 2013.

KOI	Comp.	Ang.Sep. arcsec	Angle deg.	SDSSi mag	SDSSz mag	Δi mag	Δz mag	$i-z$ mag	SpT	Season	Others[a]
					Active KOIs						
111	A	0.0	0.0	12.38 ± 0.10	–	0.0	–	–	$G0^{G5}_{F8}$	2013	H,A,L
111	B	1.856 ± 0.018	186.11 ± 0.50	18.47 ± 0.54	–	−6.095 ± 0.526	–	–	–	2013	L
115	A	0.0	0.0	12.59 ± 0.10	–	0.0	–	–	$F8^{G2}_{F5}$	2013	A,L
115	B	4.051 ± 0.039	337.43 ± 0.50	20.59 ± 1.50	–	−7.997 ± 2.251	–	–	–	2013	A,L
152	A	0.0	0.0	13.69 ± 0.10	–	0.0	–	–	$G0^{G5}_{F8}$	2013	L
152	B	5.721 ± 0.056	340.17 ± 0.50	17.14 ± 0.23	–	−3.443 ± 0.044	–	–	–	2013	–
152	C	5.721 ± 0.056	340.17 ± 0.50	17.14 ± 0.23	–	−3.443 ± 0.044	–	–	–	2013	–
191	A	0.0	0.0	14.76 ± 0.10	14.69 ± 0.10	0.0	0.0	0.0700 ± 0.141	$G8^{K0}_{G8}$	2013	L
191	B	1.671 ± 0.016	276.09 ± 0.50	17.50 ± 0.10	17.74 ± 0.11	−2.746 ± 0.023	−3.049 ± 0.038	−0.233 ± 0.148	$A1^{A9}_{B1}$	2013	L
435	A	0.0	0.0	14.27 ± 0.10	–	0.0	–	–	$G8^{K0}_{G5}$	2013	L
435	B	4.850 ± 0.047	34.75 ± 0.50	16.05 ± 0.14	–	−1.779 ± 0.009	–	–	–	2013	–
650	A	0.0	0.0	13.23 ± 0.10	–	0.000 ± 0.028	–	–	$K2^{K2}_{K1}$	2013	L
650	B	2.594 ± 0.025	88.09 ± 0.50	17.87 ± 0.59	–	−4.638 ± 0.584	–	–	–	2013	–
1174	A	0.0	0.0	12.91 ± 0.10	–	0.0	–	–	$K5^{K5}_{K4}$	2013	–
1174	B	5.060 ± 0.049	237.48 ± 0.50	17.45 ± 0.34	–	−4.541 ± 0.103	–	–	–	2013	–
1230	A	0.0	0.0	11.83 ± 0.10	–	0.0	–	–	$K3^{K3}_{K2}$	2013	L
1230	B	2.814 ± 0.027	289.07 ± 0.50	20.94 ± 7.21	–	−9.108 ± 7.206	–	–	–	2013	–
1452	A	0.0	0.0	13.46 ± 0.10	–	0.0	–	–	$F8^{G0}_{F5}$	2012	L
1452	B	2.371 ± 0.023	282.02 ± 0.57	22.75 ± 7.76	–	−9.284 ± 7.761	–	–	–	2012	–
1452	C	4.763 ± 0.046	85.26 ± 0.57	19.42 ± 0.37	–	−5.953 ± 0.361	–	–	–	2012	–
1546	A	0.0	0.0	14.57 ± 0.10	–	0.0	–	–	$K1^{K1}_{K0}$	2013	–
1546	B	0.5839 ± 0.0057	268.80 ± 0.50	15.55 ± 0.10	–	−0.987 ± 0.006	–	–	–	2013	–
1546	C	2.901 ± 0.028	3.22 ± 0.50	18.08 ± 0.11	–	−3.515 ± 0.042	–	–	–	2013	–
1546	D	4.113 ± 0.040	344.16 ± 0.50	18.21 ± 0.11	–	−3.648 ± 0.047	–	–	–	2013	–
1546	E	4.615 ± 0.045	198.72 ± 0.50	21.12 ± 0.68	–	−6.557 ± 0.669	–	–	–	2013	–
1725	A	0.0	0.0	13.95 ± 0.10	–	0.0	–	–	–	2013	L
1725	B	4.093 ± 0.040	278.31 ± 0.50	15.79 ± 0.14	–	−1.837 ± 0.010	–	–	–	2013	–
1781	A	0.0	0.0	11.81 ± 0.10	–	0.000 ± 0.001	–	–	$K2^{K3}_{K2}$	2012	L
1781	B	3.447 ± 0.033	152.14 ± 0.57	15.46 ± 0.22	–	−3.653 ± 0.037	–	–	–	2012	–
1802	A	0.0	0.0	13.11 ± 0.10	–	0.0	–	–	$G2^{G5}_{F8}$	2013	L
1802	B	5.446 ± 0.053	239.86 ± 0.50	19.58 ± 0.72	–	−6.469 ± 0.511	–	–	–	2013	–
1812	A	0.0	0.0	13.54 ± 0.10	–	0.0	–	–	$G2^{G8}_{F8}$	2013	L
1812	B	2.368 ± 0.023	117.19 ± 0.50	17.81 ± 0.13	–	−4.269 ± 0.086	–	–	–	2013	–
1812	C	2.695 ± 0.026	294.07 ± 0.50	20.05 ± 0.68	–	−6.512 ± 0.677	–	–	–	2013	–
2324	A	0.0	0.0	13.96 ± 0.10	–	0.0	–	–	–	2012	–
2324	B	2.910 ± 0.028	28.42 ± 0.57	20.08 ± 0.71	–	−6.123 ± 0.707	–	–	–	2012	–
2324	C	4.781 ± 0.046	353.04 ± 0.57	13.78 ± 0.10	–	0.180 ± 0.004	–	–	–	2012	–
2324	D	5.576 ± 0.054	89.99 ± 0.57	19.00 ± 0.28	–	−5.039 ± 0.261	–	–	–	2012	–
2481	A	0.0	0.0	13.17 ± 0.10	13.02 ± 0.10	0.0	0.0	0.150 ± 0.141	$K4^{K5}_{K4}$	2012	L
2481	B	1.097 ± 0.011	183.16 ± 0.57	16.68 ± 0.11	16.34 ± 0.10	−3.505 ± 0.039	−3.326 ± 0.031	0.329 ± 0.150	$K8^{M2}_{K5}$	2012	–
3158	A	0.0	0.0	14.03 ± 0.10	14.04 ± 0.10	0.0	0.0	−0.0100 ± 0.141	$F4^{K4}_{A4}$	2013	–
3158	B	1.845 ± 0.018	252.17 ± 0.50	16.90 ± 0.10	16.59 ± 0.10	−2.870 ± 0.021	−2.547 ± 0.018	0.313 ± 0.144	$K8^{M1}_{K5}$	2013	–
3263	A	0.0	0.0	15.31 ± 0.10	–	0.0	–	–	–	2013	–
3263	B	0.8260 ± 0.0081	94.52 ± 0.50	17.33 ± 0.10	–	−2.019 ± 0.012	–	–	–	2013	–
3444	A	0.0	0.0	12.92 ± 0.10	12.57 ± 0.10	0.0	0.0	0.350 ± 0.141	$K8^{M2}_{K5}$	2013	–
3444	B	1.080 ± 0.010	9.62 ± 0.50	15.72 ± 0.10	15.14 ± 0.10	−2.795 ± 0.021	−2.567 ± 0.019	0.578 ± 0.144	$M2^{M4}_{M0}$	2013	–
3444	C	3.579 ± 0.035	264.38 ± 0.50	17.42 ± 0.14	17.30 ± 0.17	−4.501 ± 0.100	−4.729 ± 0.141	0.122 ± 0.223	$K3^{K8}_{A7}$	2013	–
3649	A	0.0	0.0	15.82 ± 0.10	–	0.000 ± 0.020	–	–	–	2013	–
3649	B	0.6649 ± 0.0065	214.19 ± 0.50	15.97 ± 0.11	–	−0.154 ± 0.022	–	–	–	2013	–

Notes. [a] Identifier of papers that have detected the KOI and/or the companion: H for Howell et al. (2011), A for Adams et al. (2012), and L for Law et al. (2013).

Table 3. continued.

KOI	Comp.	Ang.Sep. arcsec	Angle deg.	SDSSi mag	SDSSz mag	Δi mag	Δz mag	$i-z$ mag	SpT	Season	Others[a]
3886	A	0.0	0.0	9.79 ± 0.10	9.62 ± 0.10	0.0	0.0	0.170 ± 0.141	$K4^{K4}_{K4}$	2013	–
3886	B	0.4080 ± 0.0040	294.58 ± 0.50	10.65 ± 0.10	10.61 ± 0.10	−0.854 ± 0.004	−0.986 ± 0.004	0.0380 ± 0.141	$F8^{K5}_{A7}$	2013	–
4016	A	0.0	0.0	13.51 ± 0.10	–	0.0	–	–	$K5^{K5}_{K5}$	2013	–
4016	B	5.583 ± 0.054	34.90 ± 0.50	17.47 ± 0.25	–	−3.958 ± 0.054	–	–	$M7^{M7}_{M6}$	2013	–
4512	A	0.0	0.0	15.37 ± 0.10	–	0.000 ± 0.008	–	–	$K3^{K4}_{K2}$	2013	–
4512	B	0.3922 ± 0.0038	147.99 ± 0.50	16.10 ± 0.10	–	−0.728 ± 0.011	–	–	–	2013	–
					Demoted KOIs						
3564	A	0.0	0.0	13.95 ± 0.10	–	0.0	–	–	–	2013	–
3564	B	4.912 ± 0.048	282.03 ± 0.50	16.95 ± 0.19	–	−3.002 ± 0.025	–	–	–	2013	–
3616	A	0.0	0.0	14.91 ± 0.10	14.94 ± 0.10	0.0	0.0	−0.0300 ± 0.141	$F2^{K1}_{A2}$	2013	–
3616	B	1.276 ± 0.012	212.33 ± 0.50	14.53 ± 0.10	14.50 ± 0.10	0.376 ± 0.010	0.445 ± 0.014	0.0390 ± 0.142	$G0^{K5}_{A7}$	2013	–
3639	A	0.0	0.0	13.95 ± 0.10	13.95 ± 0.10	0.0	0.0	−−	–	2013	–
3639	B	3.281 ± 0.032	37.91 ± 0.50	15.61 ± 0.13	15.79 ± 0.15	−1.661 ± 0.007	−1.842 ± 0.011	−0.181 ± 0.142	$A2^{F1}_{B3}$	2013	–
3639	C	4.601 ± 0.045	290.25 ± 0.50	15.74 ± 0.14	15.89 ± 0.15	−1.792 ± 0.008	−1.950 ± 0.012	−0.158 ± 0.142	$A3^{F3}_{B4}$	2013	–
3670	A	0.0	0.0	–	14.12 ± 0.10	–	0.0	–	–	2013	–
3670	B	1.299 ± 0.013	297.65 ± 0.50	–	16.22 ± 0.10	–	−2.107 ± 0.011	–	–	2013	–
3670	C	1.897 ± 0.018	272.89 ± 0.50	–	18.01 ± 0.11	–	−3.892 ± 0.055	–	–	2013	–
3670	D	4.822 ± 0.047	242.77 ± 0.50	–	20.56 ± 0.58	–	−6.441 ± 0.575	–	–	2013	–
3684	A	0.0	0.0	13.95 ± 0.10	13.95 ± 0.10	0.0	0.0	–	$F7^{K4}_{A5}$	2013	–
3684	B	3.755 ± 0.037	233.00 ± 0.50	19.50 ± 0.48	19.07 ± 0.48	−5.551 ± 0.221	−5.130 ± 0.222	0.421 ± 0.344	$M0^{M4}_{G2}$	2013	–
3684	C	4.102 ± 0.040	38.97 ± 0.50	21.69 ± 1.29	21.40 ± 1.38	−7.740 ± 1.656	−7.452 ± 1.882	0.288 ± 2.511	$K7^{---}_{---}$	2013	–
3693	A	0.0	0.0	13.95 ± 0.10	–	0.0	–	–	–	2013	–
3693	B	4.275 ± 0.042	205.37 ± 0.50	20.43 ± 1.13	–	−6.475 ± 1.269	–	–	–	2013	–
3704	A	0.0	0.0	14.10 ± 0.10	–	0.0	–	–	–	2013	–
3704	B	1.533 ± 0.015	137.43 ± 0.50	16.83 ± 0.10	–	−2.730 ± 0.022	–	–	–	2013	–
3704	C	2.865 ± 0.028	102.98 ± 0.50	17.02 ± 0.10	–	−2.914 ± 0.026	–	–	–	2013	–
3704	D	4.164 ± 0.041	302.78 ± 0.50	16.69 ± 0.10	–	−2.586 ± 0.019	–	–	–	2013	–
3712	A	0.0	0.0	13.95 ± 0.10	–	0.0	–	–	–	2013	–
3712	B	5.829 ± 0.057	141.51 ± 0.50	14.59 ± 0.15	–	−0.640 ± 0.013	–	–	–	2013	–
3714	A	0.0	0.0	13.95 ± 0.10	–	0.0	–	–	–	2013	–
3714	B	4.761 ± 0.046	224.26 ± 0.50	19.36 ± 0.45	–	−5.408 ± 0.196	–	–	–	2013	–
3719	A	0.0	0.0	14.38 ± 0.10	–	0.0	–	–	–	2013	–
3719	B	1.226 ± 0.012	81.99 ± 0.50	15.18 ± 0.10	–	−0.797 ± 0.013	–	–	–	2013	–
3777	A	0.0	0.0	13.99 ± 0.10	–	0.0	–	–	–	2013	–
3777	B	1.687 ± 0.016	186.36 ± 0.50	18.47 ± 0.15	–	−4.485 ± 0.110	–	–	–	2013	–
3777	C	1.884 ± 0.018	257.21 ± 0.50	18.61 ± 0.16	–	−4.621 ± 0.124	–	–	–	2013	–
3788	A	0.0	0.0	13.96 ± 0.10	–	0.0	–	–	–	2013	–
3788	B	2.263 ± 0.022	67.85 ± 0.50	19.41 ± 0.24	–	−5.451 ± 0.213	–	–	–	2013	–
3805	A	0.0	0.0	13.95 ± 0.10	–	0.0	–	–	–	2013	–
3805	B	3.684 ± 0.036	199.67 ± 0.50	19.43 ± 0.53	–	−5.474 ± 0.274	–	–	–	2013	–
3805	C	4.389 ± 0.043	105.00 ± 0.50	16.52 ± 0.17	–	−2.572 ± 0.019	–	–	–	2013	–
3842	A	0.0	0.0	13.95 ± 0.10	–	0.0	–	–	–	2013	–
3842	B	3.684 ± 0.036	247.05 ± 0.50	15.50 ± 0.15	–	−1.552 ± 0.013	–	–	–	2013	–
3940	A	0.0	0.0	13.97 ± 0.10	–	0.0	–	–	–	2013	–
3940	B	2.132 ± 0.021	256.74 ± 0.50	18.76 ± 0.17	–	−4.792 ± 0.141	–	–	–	2013	–
4013	A	0.0	0.0	14.27 ± 0.10	14.22 ± 0.10	0.0	0.0	0.0500 ± 0.141	$G1^{K5}_{A8}$	2013	–
4013	B	0.9166 ± 0.0089	62.14 ± 0.50	15.43 ± 0.10	15.58 ± 0.10	−1.157 ± 0.005	−1.367 ± 0.005	−0.160 ± 0.141	$A2^{F2}_{B4}$	2013	–
4033	A	0.0	0.0	14.04 ± 0.10	14.03 ± 0.10	0.0	0.0	0.0100 ± 0.141	$F7^{K4}_{A5}$	2013	–
4033	B	1.617 ± 0.016	290.55 ± 0.50	16.86 ± 0.10	16.89 ± 0.10	−2.823 ± 0.021	−2.865 ± 0.026	−0.0320 ± 0.145	$F2^{K1}_{A2}$	2013	–
4033	C	2.925 ± 0.028	96.42 ± 0.50	19.58 ± 0.28	19.58 ± 0.32	−5.548 ± 0.261	−5.551 ± 0.305	0.00700 ± 0.425	$F7^{M0}_{O7}$	2013	–
4355	A	0.0	0.0	14.48 ± 0.10	–	0.0	–	–	–	2013	–
4355	B	2.864 ± 0.028	273.15 ± 0.50	14.99 ± 0.10	–	−0.516 ± 0.004	–	–	–	2013	–

Table 4. Sensitivity limit results (at 5σ level) for all observed targets (230 KOIs) in the 2011, 2012, and 2013 observing seasons.

KOI	Others[a]	Filter	m^b	Δm at 0.2″	Δm at 0.5″	Δm at 1.0″	Δm at 2.0″	Δm at 3.0″
Active KOIs								
12	L	*i*	11.19	1.99	3.58	4.20	3.40	4.50
41	H, A, L	*i*	10.98	0.08	2.32	5.64	8.55	8.71
49	H,L	*i*	13.46	0.75	3.61	6.78	8.11	6.83
51	–	*i*	13.98	1.11	3.22	5.93	7.64	6.50
69	H, A, L	*i*	9.69	2.50	1.46	4.87	7.82	9.00
82	H, A, L	*i*	11.11	0.87	2.74	5.28	8.17	8.83
94	H, A, L	*i*	12.01	1.52	2.88	4.64	7.05	7.72
99	L	*i*	12.64	1.08	3.91	6.96	7.57	6.20
111	H, A, L	*i*	12.39	1.28	3.12	5.37	7.51	7.90
115	A, L	*i*	12.60	1.16	3.16	5.38	7.41	7.00
131	L	*i*	13.59	0.62	3.26	5.91	7.17	6.83
139	L	*i*	13.28	0.69	3.16	5.74	7.05	6.36
149	L	*i*	13.12	0.75	3.36	5.36	7.15	6.00
152	L	*i*	13.71	1.25	3.62	6.54	6.89	5.60
156	L	*i*	13.30	1.25	3.13	5.49	6.72	5.17
191	L	*i*	14.70	1.75	3.79	5.92	5.35	4.67
191	L	*z*	14.63	1.25	4.22	6.15	4.71	4.31
196	H	*i*	14.19	1.50	3.08	4.99	5.28	6.00
199	–	*i*	14.67	0.58	3.42	5.55	6.93	7.17
209	L	*i*	14.08	0.58	3.52	6.02	6.42	5.33
211	L	*i*	14.77	2.05	3.91	5.69	5.62	4.42
212	–	*i*	14.61	1.14	3.79	5.70	5.53	4.50
232	L	*i*	14.02	0.69	2.95	5.61	7.10	7.75
238	L	*i*	13.84	1.14	3.64	6.74	7.28	5.78
245	H, A	*i*	–	1.00	3.03	5.79	8.64	9.14
298	–	*i*	12.32	1.38	2.62	4.49	6.39	7.38
298	–	*z*	–	0.75	3.02	6.14	6.53	7.75
326	–	*i*	†12.96	0.75	3.24	5.05	6.68	6.71
330	L	*i*	13.68	1.15	3.55	6.66	7.46	6.22
338	–	*i*	13.07	0.75	3.17	5.26	6.72	7.50
338	–	*z*	12.95	0.64	3.18	4.78	6.93	7.10
339	L	*i*	13.56	0.62	3.42	6.67	6.65	6.17
343	L	*i*	12.96	2.11	2.88	5.77	6.69	8.36
345	L	*i*	12.96	2.09	4.14	4.68	4.53	5.25
346	–	*z*	13.07	1.64	3.32	4.74	6.01	6.67
349	L	*i*	13.33	0.69	2.83	5.33	6.36	7.90
351	–	*i*	13.61	1.25	3.03	4.40	4.80	6.50
366	H, L	*i*	–	0.14	3.35	5.90	5.73	8.50
372	H, A, L	*i*	12.16	0.72	3.23	5.19	6.41	7.25
372	H, A, L	*z*	12.11	0.69	3.35	5.64	6.76	7.00
375	–	*i*	13.06	0.72	2.94	5.61	5.72	7.25
379	–	*i*	13.13	1.11	3.21	5.23	6.91	7.36
379	–	*z*	13.03	0.75	3.41	5.59	7.25	6.50
385	L	*i*	13.16	8.50	5.21	4.45	3.59	4.83
386	L	*i*	13.61	1.50	2.93	4.65	6.05	6.67
387	–	*i*	13.19	0.96	3.08	5.59	5.71	8.08
387	–	*z*	–	0.58	3.23	4.55	7.05	7.33
388	L	*i*	13.40	0.75	3.00	4.34	6.27	6.50
393	L	*i*	13.34	1.21	3.37	5.66	6.51	7.92
398	H	*i*	15.00	2.50	3.79	6.33	5.44	4.81
401	L	*i*	13.69	0.64	2.77	5.81	7.54	7.86
401	L	*z*	13.59	0.89	3.31	6.30	7.16	7.36
408	L	*i*	14.72	2.71	4.57	5.33	6.26	5.70
416	L	*i*	13.97	1.25	3.70	6.20	7.04	6.70
422	–	*i*	14.51	1.57	3.86	3.88	3.39	7.62
422	–	*z*	14.45	1.59	4.30	6.36	5.63	7.00
431	L	*i*	13.96	1.62	3.33	5.41	6.95	5.33
433	–	*i*	14.58	1.25	3.65	5.55	6.39	5.92
433	–	*z*	14.48	1.25	3.52	5.30	6.38	7.08

Notes. The sensitivity limits at the different angular separations (Δm, Cols. 5 to 9) are provided in the corresponding *i* and *z* bands (Col. 3). [(a)] Identifier of papers where high-resolution images are provided for each KOI: H for Howell et al. (2011), A for Adams et al. (2012), and L for Law et al. (2013). [(b)] Magnitude in the SDSS filter system of the corresponding band (in previous column) obtained by transforming the KIC magnitudes with equations provided by Pinsonneault et al. (2012). † KIC magnitude that was not converted to the SDSS system due to the lack of some needed magnitudes in Eqs. (3) and (4) of Pinsonneault et al. (2012).

Table 4. continued.

KOI	Others[a]	Filter	m^b	Δm at 0.2″	Δm at 0.5″	Δm at 1.0″	Δm at 2.0″	Δm at 3.0″
435	L	*i*	14.29	0.69	3.70	6.35	5.92	5.00
439	L	*i*	14.02	1.25	3.00	5.02	6.52	6.80
463	L	*i*	14.00	1.74	3.48	5.55	6.69	5.83
465	L	*i*	13.97	1.52	3.26	5.81	6.33	5.33
473	–	*i*	14.39	2.28	3.97	5.26	6.29	6.70
478	L	*i*	13.59	0.72	2.78	5.43	4.95	7.50
481	L	*i*	14.40	1.90	3.78	5.52	6.01	4.67
490	L	*i*	13.65	5.75	7.05	5.67	6.11	6.42
496	–	*i*	14.09	0.75	3.04	5.17	6.25	7.50
518	–	*i*	13.94	0.75	3.33	6.04	6.35	5.28
520	L	*i*	14.21	1.25	2.96	4.82	4.84	6.80
524	–	*i*	14.56	2.23	4.01	5.43	5.68	4.36
528	L	*i*	14.32	2.64	4.22	5.24	6.47	4.80
534	L	*i*	14.30	0.83	3.14	5.00	4.00	6.92
548	L	*i*	13.82	0.50	2.80	4.78	6.24	7.62
555	A, L	*i*	14.45	0.72	3.21	5.40	7.00	7.08
561	L	*i*	13.69	1.47	2.93	4.79	5.09	6.79
564	L	*i*	14.60	1.74	3.68	5.78	6.02	5.38
567	L	*i*	14.08	1.45	2.87	5.19	6.28	7.14
571	L	*i*	14.00	1.08	3.52	5.26	6.16	6.36
579	L	*i*	13.81	2.50	3.52	6.36	7.36	5.81
589	–	*i*	14.33	1.24	3.77	6.73	6.58	5.70
592	–	*i*	14.05	1.25	3.42	4.97	6.46	6.75
592	–	*z*	13.97	2.09	3.67	5.27	5.82	6.38
611	L	*i*	13.81	0.83	2.75	5.11	6.74	7.33
617	–	*i*	14.34	1.67	3.39	5.78	6.23	4.86
623	H, L	*i*	11.63	0.00	3.61	5.64	6.92	8.83
624	L	*i*	13.34	1.46	3.03	5.30	7.15	5.75
625	L	*i*	13.38	0.58	3.23	5.80	6.36	5.10
626	L	*i*	13.29	0.69	3.09	4.56	5.84	6.83
626	L	*z*	13.24	0.83	3.25	5.06	6.35	6.50
628	L	*i*	13.70	0.75	2.88	4.97	5.48	6.33
628	L	*z*	13.62	1.72	3.51	4.65	4.85	6.50
632	L	*i*	13.08	0.25	2.77	5.83	5.73	4.70
638	A, L	*i*	13.35	0.75	3.05	5.15	6.63	7.31
640	L	*i*	13.01	5.74	5.88	4.47	6.33	6.50
641	–	*i*	13.04	0.75	3.03	5.32	6.38	7.33
641	–	*z*	12.71	1.25	3.16	5.25	6.20	5.67
644	L	*i*	13.43	0.64	3.09	4.83	6.26	7.38
644	L	*z*	13.33	0.75	3.23	5.56	6.82	7.50
645	–	*i*	13.49	1.20	3.43	6.52	7.58	8.08
645	–	*z*	13.42	0.64	3.51	6.47	6.57	5.31
650	L	*i*	13.25	1.25	3.53	4.32	4.14	1.75
654	L	*i*	13.74	1.59	3.23	5.67	6.29	4.92
658	L	*i*	13.74	0.69	2.82	5.74	5.94	7.62
658	L	*z*	13.65	0.83	3.11	5.24	5.53	7.00
659	L	*i*	13.24	0.42	3.17	6.29	8.07	6.67
664	L	*i*	13.24	1.25	3.97	6.91	8.26	7.60
670	–	*i*	13.51	0.25	3.62	6.70	7.53	8.50
671	L	*i*	13.47	0.75	2.73	5.29	6.88	8.12
672	–	*i*	13.72	5.11	8.05	6.62	4.68	6.25
676	L	*i*	13.34	0.83	3.24	5.36	7.07	7.58
678	–	*i*	12.95	0.94	3.17	5.68	7.30	8.00
682	L	*i*	13.65	1.74	3.50	5.80	6.44	4.78
684	L	*i*	13.53	1.38	3.21	5.86	6.55	5.17
685	L	*i*	13.72	0.83	3.05	6.13	7.39	7.75
685	L	*z*	13.71	0.62	3.26	6.14	7.01	6.90
686	L	*i*	13.30	0.75	3.17	5.77	6.95	5.50
693	–	*i*	13.75	0.64	3.24	5.86	7.33	5.92
695	L	*i*	13.23	1.22	3.08	4.37	5.12	6.33
703	L	*i*	13.11	1.38	3.82	6.28	7.12	7.75
703	L	*z*	–	0.97	3.31	6.20	7.31	7.62
704	L	*i*	13.41	0.83	3.20	5.28	6.41	7.25
709	L	*i*	13.67	1.23	3.48	6.47	7.51	6.14

Table 4. continued.

KOI	Others[a]	Filter	m^b	Δm at 0.2″	Δm at 0.5″	Δm at 1.0″	Δm at 2.0″	Δm at 3.0″
717	L	*i*	13.13	2.00	3.78	6.70	7.97	8.22
721	L	*i*	13.39	1.20	3.84	7.04	8.09	7.81
721	L	*z*	13.34	2.50	3.64	6.36	7.11	7.22
739	L	*i*	14.91	1.70	3.47	5.11	6.12	6.28
800	L	*i*	15.29	1.75	3.55	4.18	4.23	4.22
800	L	*z*	15.21	1.08	4.07	5.00	5.68	5.83
834	L	*i*	14.81	1.70	3.80	6.36	5.61	4.86
841	–	*i*	15.53	0.69	3.78	6.22	6.54	5.78
841	–	*z*	15.44	1.72	4.01	5.62	5.46	5.31
881	–	*i*	15.52	0.69	3.79	5.81	6.53	6.79
884	L	*i*	14.71	2.34	4.01	5.65	5.71	4.36
1032	L	*i*	13.46	1.42	2.84	4.26	6.17	7.50
1096	–	*i*	14.43	1.67	3.55	5.54	6.14	4.86
1174	–	*i*	12.97	1.20	3.23	5.97	7.62	6.25
1192	–	*i*	13.92	0.25	2.79	5.57	7.78	8.21
1230	L	*i*	11.88	1.09	3.23	5.87	7.92	7.25
1236	L	*i*	13.46	1.25	3.39	4.87	6.72	6.83
1268	–	*i*	14.59	1.22	3.40	5.39	6.56	5.00
1353	L	*i*	13.72	0.75	3.30	6.03	6.86	5.25
1356	–	*i*	14.93	2.11	3.88	5.66	5.65	4.42
1375	L	*i*	13.48	1.23	3.22	6.39	7.59	7.00
1375	L	*z*	–	0.75	2.98	6.24	6.88	6.62
1376	L	*i*	13.85	2.21	3.73	5.02	6.28	6.60
1421	–	*i*	15.04	1.19	3.77	5.94	5.58	4.75
1426	L	*i*	14.01	0.75	3.35	5.85	6.64	5.31
1452	L	*i*	13.47	0.72	3.20	5.73	6.77	5.50
1477	–	*i*	15.61	1.14	4.01	6.22	5.25	4.81
1527	–	*i*	14.58	2.18	4.03	5.62	5.83	4.42
1529	L	*i*	14.10	2.29	4.10	5.56	5.56	4.31
1546	–	*i*	14.19	1.67	3.27	5.93	6.88	6.67
1573	–	*i*	14.14	1.25	2.92	4.70	5.81	6.90
1574	–	*i*	14.33	0.75	3.58	6.60	6.41	5.36
1596	L	*i*	14.72	2.22	4.02	5.60	5.85	4.42
1684	L	*i*	12.66	0.75	2.95	5.03	7.12	6.83
1701	L	*i*	10.99	0.95	2.94	5.96	7.89	6.75
1725	L	*i*	13.07	1.23	3.74	6.53	8.42	7.12
1779	L	*i*	13.03	0.83	3.08	5.82	7.39	6.38
1781	L	*i*	11.85	0.64	2.81	4.67	7.00	7.17
1800	–	*i*	12.13	0.75	3.04	4.92	7.41	7.50
1802	L	*i*	13.12	1.67	3.05	5.08	7.16	5.42
1805	L	*i*	13.54	0.58	3.19	6.12	6.85	5.58
1812	L	*i*	13.53	0.75	3.30	5.81	7.19	5.50
1894	L	*i*	13.01	2.50	3.29	6.03	7.88	6.38
1925	L	*i*	9.16	0.14	2.82	5.82	8.67	9.30
2042	L	*i*	12.89	0.75	2.97	5.19	7.05	7.67
2133	L	*i*	12.07	1.17	3.23	5.89	8.31	8.00
2260	L	*i*	12.00	1.00	3.13	6.16	7.30	6.12
2324	–	*i*	11.26	1.25	2.91	3.07	4.74	7.70
2352	L	*i*	–	0.22	3.18	6.44	8.68	8.86
2481	L	*i*	13.18	1.17	3.42	6.28	7.37	6.00
2481	L	*z*	12.97	0.58	3.25	6.17	7.20	6.38
2545	L	*i*	11.57	1.17	3.36	6.55	8.66	8.75
2593	L	*i*	–	1.17	3.07	5.74	8.28	8.12
2632	L	*i*	11.22	1.54	3.35	5.45	6.32	4.92
2640	L	*i*	12.86	1.09	3.29	5.98	8.10	6.90
2674	–	*i*	13.11	1.22	3.36	6.37	7.76	6.50
2712	–	*i*	10.96	0.22	2.73	5.18	7.83	9.00
3158	–	*i*	–	0.22	2.88	5.44	7.63	8.28
3158	–	*z*	–	0.89	3.20	6.08	7.92	8.31
3179	–	*i*	10.49	2.50	2.88	5.04	7.73	8.22
3203	–	*i*	11.67	1.25	2.94	4.61	7.21	8.12
3206	–	*i*	11.56	1.70	3.07	4.31	6.52	7.25
3237	–	*i*	12.09	0.58	2.71	5.08	7.78	7.67
3263	–	*i*	15.27	1.88	4.18	5.97	5.71	5.31
3444	–	*i*	12.98	1.01	3.46	6.38	7.66	6.71

Table 4. continued.

KOI	Others[a]	Filter	m^b	Δm at 0.2″	Δm at 0.5″	Δm at 1.0″	Δm at 2.0″	Δm at 3.0″
3444	–	*z*	12.48	1.28	3.82	6.81	7.65	6.78
3554	–	*i*	14.94	1.08	3.88	5.32	6.56	6.33
3560	–	*i*	11.64	1.23	3.21	5.58	7.97	6.50
3649	–	*i*	15.17	1.43	5.77	5.98	6.57	6.28
3692	–	*z*	14.73	2.32	5.95	7.93	6.64	5.83
3728	–	*i*	12.14	0.72	3.07	5.04	7.18	6.50
3742	–	*i*	14.77	0.25	2.85	4.96	6.37	8.50
3765	–	*i*	16.00	2.34	4.56	5.91	4.68	4.28
3765	–	*z*	15.73	1.22	4.52	5.78	4.34	4.40
3801	–	*i*	15.71	1.14	4.44	6.04	4.47	4.36
3853	–	*i*	10.28	0.12	3.03	5.54	8.41	8.75
3886	–	*i*	9.43	1.14	4.49	4.99	8.01	8.86
3886	–	*z*	9.26	0.99	2.89	5.52	8.21	9.25
3890	–	*i*	12.83	1.50	4.33	6.97	8.40	7.00
3925	–	*i*	13.74	0.64	3.43	6.21	6.92	5.67
4016	–	*i*	13.57	1.54	3.16	5.48	6.54	5.17
4351	–	*i*	14.67	0.33	3.52	6.21	5.65	4.88
4512	–	*i*	14.97	5.57	8.25	5.71	6.22	5.86
				Demoted KOIs				
6	–	*i*	11.99	0.75	3.24	5.74	7.12	5.64
1187	–	*i*	14.21	0.75	3.40	6.11	6.01	5.10
1924	L	*i*	7.62	0.00	2.70	5.27	8.32	9.28
3157	–	*i*	8.27	2.00	2.97	5.84	7.25	7.42
3178	–	*i*	10.46	0.14	3.33	6.55	8.71	9.70
3564	–	*i*	14.16	0.19	2.73	5.57	7.86	8.12
3570	–	*i*	14.80	0.75	3.20	4.87	6.76	7.25
3571	–	*i*	15.24	0.50	2.99	5.01	7.00	8.17
3588	–	*i*	15.96	4.75	4.43	4.81	6.22	6.50
3597	–	*i*	14.09	1.71	3.50	5.60	6.26	6.36
3616	–	*i*	15.45	4.14	5.53	5.45	5.89	2.83
3616	–	*z*	15.23	3.83	5.51	5.72	4.87	4.60
3633	–	*z*	–	1.57	5.28	4.37	5.89	5.92
3639	–	*z*	12.84	0.62	3.60	6.25	7.06	5.83
3639	–	*i*	13.05	0.75	3.38	5.27	7.23	6.75
3658	–	*i*	15.08	7.83	6.54	5.52	6.32	6.10
3670	–	*z*	12.23	2.50	3.71	6.18	7.30	7.21
3684	–	*i*	12.11	0.58	3.23	4.76	5.48	7.83
3684	–	*z*	12.10	0.33	3.48	6.76	8.47	7.33
3693	–	*i*	14.27	1.54	4.16	6.42	6.14	5.14
3704	–	*i*	16.99	2.21	4.25	6.47	6.58	6.38
3706	–	*i*	14.39	1.97	3.79	5.58	6.40	6.17
3712	–	*i*	16.47	2.86	5.14	6.02	4.42	3.92
3714	–	*i*	14.94	0.75	3.06	5.05	7.41	7.50
3719	–	*i*	15.81	1.08	3.97	5.50	6.28	5.50
3719	–	*i*	15.81	1.57	4.89	6.18	5.36	6.14
3723	–	*i*	9.93	0.62	2.19	3.08	3.92	6.00
3725	–	*i*	9.69	1.18	3.21	5.76	8.50	9.22
3727	–	*i*	15.30	1.94	5.68	7.30	7.65	6.50
3730	–	*i*	18.48	1.81	3.78	5.16	6.51	6.50
3744	–	*i*	15.41	1.50	4.19	6.50	5.63	4.81
3763	–	*i*	17.04	2.46	4.12	5.00	6.59	6.75
3777	–	*i*	11.52	0.14	3.26	6.37	8.41	7.70
3788	–	*i*	8.88	0.56	2.78	5.13	8.03	9.29
3793	–	*i*	16.13	1.97	5.68	5.96	4.53	4.75
3795	–	*i*	14.56	0.64	3.06	4.78	6.43	7.80
3796	–	*i*	12.29	0.72	3.07	5.10	7.46	6.75
3800	–	*i*	17.01	3.20	6.14	7.13	5.21	5.00
3803	–	*i*	13.40	1.26	3.61	6.42	7.69	6.12
3805	–	*i*	10.92	0.25	3.29	6.16	8.22	8.75
3810	–	*i*	16.10	2.39	4.64	6.14	4.64	4.62
3814	–	*i*	12.46	1.21	3.43	6.19	8.00	6.10
3817	–	*i*	16.10	1.72	3.76	6.11	5.17	4.70
3821	–	*i*	16.50	1.12	3.03	4.82	7.42	8.19

Table 4. continued.

KOI	Others[a]	Filter	m^b	Δm at 0.2″	Δm at 0.5″	Δm at 1.0″	Δm at 2.0″	Δm at 3.0″
3824	–	*i*	15.64	2.80	5.00	6.09	5.13	4.42
3827	–	*i*	15.09	1.25	4.09	5.90	5.17	4.28
3842	–	*i*	16.95	2.57	4.76	6.08	6.09	5.79
3845	–	*i*	13.33	1.20	3.70	6.83	7.41	6.00
3849	–	*i*	15.50	2.38	4.38	5.97	5.17	4.42
3873	–	*i*	10.09	0.22	3.20	6.39	8.76	8.81
3919	–	*i*	12.61	1.25	3.40	6.17	8.36	8.00
3940	–	*i*	12.54	1.21	3.42	6.18	8.28	7.33
3993	–	*i*	14.62	0.75	3.01	4.90	6.63	2.00
3998	–	*i*	16.76	1.42	5.03	6.06	4.35	4.42
4013	–	*i*	9.25	0.62	1.76	2.95	6.72	8.75
4013	–	*z*	9.39	0.33	2.17	4.61	7.59	6.50
4033	–	*i*	11.75	1.11	3.19	5.83	7.75	8.90
4033	–	*z*	11.70	1.15	3.56	6.60	7.51	7.12
4355	–	*i*	13.08	0.12	3.47	5.78	6.75	5.75

Table 7. Results of the blended source probability prior ($P_{BS,0}$) and after (P_{BS}^{LB14}) the AstraLux images for 222 planet candidates around isolated KOIs from all three observing runs ($Type = 0$) and KOIs with detected companions at 3–6 arcsec from the 2012 and 2013 observing runs ($Type = 1$).

Planet candidate	Type[a]	m_{kep} mag	Δm_{max} mag	$P_{BS,0}$ %	P_{BS}^{LB14} %	Improve %	P_{appEB} %	P_{BB} %
Active KOIs								
12.01	0	11.35	–4.83	1.8	0.7	61.5	0.0431	0.0003
41.01	0	11.20	–8.62	6.1	1.9	68.5	0.0404	0.0008
41.02	0	11.20	–9.77	10.1	5.8	42.1	0.0404	0.0024
41.03	0	11.20	–9.61	9.4	5.2	44.9	0.0404	0.0021
49.01	0	13.70	–7.31	8.1	3.4	57.7	0.0245	0.0008
51.01	0	13.76	–3.75	2.9	0.1	97.9	0.0241	0.0000
69.01	0	9.93	–8.45	4.1	1.5	63.7	0.0501	0.0007
82.01	0	11.49	–7.15	1.3	0.2	84.7	0.0307	0.0001
82.02	0	11.49	–8.46	2.5	1.0	60.2	0.0307	0.0003
82.03	0	11.49	–8.99	3.1	1.6	48.5	0.0307	0.0005
82.04	0	11.49	–9.73	4.2	2.7	35.7	0.0307	0.0008
82.05	0	11.49	–10.36	5.3	3.8	28.1	0.0307	0.0012
94.01	0	12.21	–5.35	3.7	0.3	90.8	0.0342	0.0001
94.02	0	12.21	–7.37	10.6	4.1	61.2	0.0342	0.0014
94.03	0	12.21	–6.44	6.8	1.2	82.2	0.0342	0.0004
94.04	0	12.21	–9.21	23.8	17.2	27.6	0.0342	0.0059
115.01	1	12.79	–7.63	4.5	1.9	57.1	0.0272	0.0005
115.02	1	12.79	–8.84	7.4	4.8	34.7	0.0272	0.0013
115.03	1	12.79	–11.03	14.8	12.2	17.5	0.0272	0.0033
139.01	0	13.49	–5.82	3.9	0.9	76.4	0.0250	0.0002
139.02	0	13.49	–9.03	15.2	12.0	21.0	0.0250	0.0030
149.01	0	13.40	–7.14	6.0	2.6	56.4	0.0253	0.0007
152.01	1	13.91	–5.98	13.6	3.3	75.7	0.0235	0.0008
152.02	1	13.91	–7.36	25.1	14.4	42.6	0.0235	0.0034
152.03	1	13.91	–7.50	26.6	16.0	40.1	0.0235	0.0038
152.04	1	13.91	–7.88	31.3	20.7	34.1	0.0235	0.0049
156.01	0	13.74	–7.72	9.9	6.2	37.3	0.0244	0.0015
156.02	0	13.74	–8.27	12.4	8.7	29.8	0.0244	0.0021
156.03	0	13.74	–6.81	6.7	3.0	55.0	0.0244	0.0007
196.01	0	14.46	–4.67	4.0	0.4	90.0	0.0234	0.0001
199.01	0	14.88	–4.72	4.8	1.0	80.2	0.0236	0.0002
199.02	0	14.88	–8.57	23.4	19.2	18.2	0.0236	0.0045
209.01	0	14.27	–5.31	2.8	0.6	79.4	0.0241	0.0001
209.02	0	14.27	–6.20	4.3	1.9	55.2	0.0241	0.0005
211.01	0	14.99	–4.99	3.1	0.6	80.0	0.0245	0.0002
238.01	0	14.06	–7.80	23.9	16.4	31.3	0.0233	0.0038
238.02	0	14.06	–9.07	39.0	31.5	19.2	0.0233	0.0074
245.01	0	9.71	–7.61	0.9	0.1	84.5	0.0444	0.0001
245.02	0	9.71	–9.53	2.3	1.3	45.9	0.0444	0.0006
245.03	0	9.71	–11.42	5.3	4.2	20.2	0.0444	0.0019
245.04	0	9.71	–10.82	4.1	3.1	26.0	0.0444	0.0014
330.01	0	13.93	–8.34	16.3	11.9	27.0	0.0239	0.0028
330.02	0	13.93	–10.20	29.0	24.6	15.2	0.0239	0.0059
338.01	0	13.45	–8.21	16.0	12.6	21.7	0.0252	0.0032
338.02	0	13.45	–9.90	29.8	26.3	11.7	0.0252	0.0066
339.01	0	13.76	–8.40	7.1	5.1	28.1	0.0246	0.0013
339.02	0	13.76	–8.44	7.2	5.2	27.7	0.0246	0.0013
339.03	0	13.76	–8.52	7.4	5.4	26.9	0.0246	0.0013
345.01	0	13.34	–6.84	3.3	2.2	33.6	0.0253	0.0005
349.01	0	13.59	–7.68	5.1	3.2	36.7	0.0248	0.0008
351.01	0	13.80	–4.93	1.4	0.1	90.5	0.0247	0.0000
351.02	0	13.80	–5.66	2.0	0.5	72.3	0.0247	0.0001
351.03	0	13.80	–7.69	4.8	3.3	31.4	0.0247	0.0008
351.04	0	13.80	–7.97	5.4	3.9	28.2	0.0247	0.0010
351.05	0	13.80	–9.07	7.8	6.3	19.5	0.0247	0.0015
351.06	0	13.80	–9.43	8.6	7.1	17.5	0.0247	0.0018
366.01	0	11.71	–5.73	2.4	0.7	69.7	0.0373	0.0003
372.01	0	12.39	–4.99	4.2	0.8	80.5	0.0330	0.0003

Notes. See Sect. 4.1 for more details. [(a)] Type = 0 for isolated KOIs (no companions within 6 arcsec from the host star) and Type = 1 for KOIs with at least one companion between 3–6 arcsec (see Table 3 for photometric information about the detected companions).

Table 7. continued.

Planet candidate	Type[a]	m_{kep} mag	Δm_{max} mag	$P_{BS,0}$ %	P_{BS}^{LB14} %	Improve %	P_{appEB} %	P_{BB} %
385.01	0	13.44	–8.38	19.0	16.1	15.1	0.0253	0.0041
386.01	0	13.84	–7.16	16.7	9.9	40.9	0.0238	0.0024
386.02	0	13.84	–7.44	18.9	12.0	36.2	0.0238	0.0029
388.01	0	13.64	–8.16	8.4	6.1	27.3	0.0247	0.0015
393.01	0	13.54	–8.34	23.6	17.4	26.3	0.0248	0.0043
398.01	0	15.34	–4.75	3.8	0.9	76.3	0.0247	0.0002
398.02	0	15.34	–6.53	8.5	5.4	36.5	0.0247	0.0013
398.03	0	15.34	–7.87	13.5	10.4	22.9	0.0247	0.0026
416.01	0	14.29	–6.62	6.0	3.1	47.6	0.0239	0.0007
416.02	0	14.29	–6.97	6.9	4.1	41.3	0.0239	0.0010
416.03	0	14.29	–9.30	15.5	12.7	18.4	0.0239	0.0030
422.01	0	14.74	–4.23	2.6	0.8	69.6	0.0239	0.0002
431.01	0	14.26	–6.99	4.0	2.4	40.1	0.0246	0.0006
431.02	0	14.26	–7.29	4.5	2.9	35.5	0.0246	0.0007
435.01	1	14.53	–6.71	5.8	3.3	43.0	0.0241	0.0008
435.02	1	14.53	–4.94	2.6	0.3	89.0	0.0241	0.0001
435.03	1	14.53	–7.66	8.5	5.9	29.8	0.0241	0.0014
435.04	1	14.53	–8.58	11.5	8.9	21.9	0.0241	0.0022
435.05	1	14.53	–7.31	7.4	4.9	33.9	0.0241	0.0012
435.06	1	14.53	–8.81	12.3	9.7	20.5	0.0241	0.0023
463.01	0	14.71	–6.12	17.9	9.0	49.5	0.0228	0.0021
473.01	0	14.67	–7.24	16.0	11.0	31.3	0.0233	0.0026
478.01	0	14.27	–6.49	10.2	6.0	41.3	0.0233	0.0014
481.01	0	14.70	–7.15	10.1	7.0	31.0	0.0238	0.0017
481.02	0	14.70	–7.98	13.8	10.6	22.8	0.0238	0.0025
481.03	0	14.70	–7.05	9.7	6.6	32.2	0.0238	0.0016
496.01	0	14.41	–7.91	14.3	10.5	26.3	0.0236	0.0025
518.01	0	14.29	–7.06	6.9	3.6	47.1	0.0240	0.0009
518.02	0	14.29	–7.60	8.5	5.3	38.0	0.0240	0.0013
518.03	0	14.29	–6.79	6.1	2.9	52.9	0.0240	0.0007
524.01	0	14.87	–7.14	6.1	4.1	31.9	0.0247	0.0010
528.01	0	14.60	–7.45	7.5	5.3	29.8	0.0242	0.0013
528.02	0	14.60	–7.10	6.6	4.3	34.1	0.0242	0.0011
528.03	0	14.60	–7.42	7.4	5.2	30.2	0.0242	0.0013
534.01	0	14.61	–7.40	19.1	14.3	25.2	0.0232	0.0033
534.02	0	14.61	–7.98	24.0	19.2	20.1	0.0232	0.0044
561.01	0	14.01	–7.78	5.8	4.2	26.9	0.0245	0.0010
564.01	0	14.85	–7.56	21.9	15.6	28.6	0.0233	0.0036
564.02	0	14.85	–5.66	9.7	3.5	63.7	0.0233	0.0008
564.03	0	14.85	–9.03	35.6	29.3	17.6	0.0233	0.0068
567.01	0	14.34	–7.43	12.7	8.6	32.2	0.0235	0.0020
567.02	0	14.34	–7.80	14.7	10.6	27.8	0.0235	0.0025
567.03	0	14.34	–7.62	13.8	9.7	29.7	0.0235	0.0023
571.01	0	14.62	–7.44	28.1	20.1	28.7	0.0229	0.0046
571.02	0	14.62	–7.25	26.0	17.9	31.1	0.0229	0.0041
571.03	0	14.62	–7.79	32.4	24.4	24.9	0.0229	0.0056
571.04	0	14.62	–7.43	27.9	19.8	28.9	0.0229	0.0045
571.05	0	14.62	–7.86	33.2	25.2	24.3	0.0229	0.0058
579.01	0	14.14	–8.21	10.7	7.8	26.9	0.0240	0.0019
579.02	0	14.14	–8.18	10.5	7.7	27.1	0.0240	0.0018
611.01	0	14.02	–5.60	11.8	2.9	75.4	0.0233	0.0007
617.01	0	14.61	–5.10	6.6	1.6	76.2	0.0232	0.0004
624.01	0	13.60	–7.35	10.8	5.2	52.3	0.0247	0.0013
624.02	0	13.60	–7.39	11.0	5.3	51.4	0.0247	0.0013
624.03	0	13.60	–8.54	17.7	12.1	31.9	0.0247	0.0030
625.01	0	13.59	–6.94	5.7	3.2	44.0	0.0248	0.0008
632.01	0	13.36	–8.52	13.0	9.9	23.8	0.0255	0.0025
638.01	0	13.60	–7.04	15.2	8.8	41.8	0.0246	0.0022
638.02	0	13.60	–6.96	14.6	8.3	43.2	0.0246	0.0020
640.01	0	13.33	–7.50	21.1	10.8	48.8	0.0259	0.0028
654.01	0	13.98	–8.21	8.4	6.5	23.2	0.0243	0.0016
654.02	0	13.98	–8.43	9.1	7.1	21.5	0.0243	0.0017
659.01	0	13.41	–8.33	15.2	10.0	34.1	0.0253	0.0025
664.01	0	13.48	–8.64	15.8	11.8	25.3	0.0251	0.0029

Table 7. continued.

Planet candidate	Type[a]	m_{kep} mag	Δm_{max} mag	$P_{BS,0}$ %	P_{BS}^{LB14} %	Improve %	P_{appEB} %	P_{BB} %
664.02	0	13.48	–9.51	21.5	17.5	18.6	0.0251	0.0044
664.03	0	13.48	–9.48	21.2	17.3	18.8	0.0251	0.0043
670.01	0	13.77	–8.46	15.9	11.5	27.8	0.0242	0.0028
672.01	0	14.00	–7.60	11.4	8.9	22.5	0.0238	0.0021
672.02	0	14.00	–7.04	9.1	6.5	28.3	0.0238	0.0015
672.03	0	14.00	–10.86	30.8	28.2	8.4	0.0238	0.0067
676.01	0	13.82	–5.90	5.5	2.0	63.5	0.0241	0.0005
676.02	0	13.82	–6.52	7.4	3.8	49.1	0.0241	0.0009
678.01	0	13.28	–8.44	7.2	5.2	27.4	0.0255	0.0013
678.02	0	13.28	–8.52	7.4	5.4	26.7	0.0255	0.0014
682.01	0	13.92	–5.35	5.8	0.8	85.4	0.0238	0.0002
684.01	0	13.83	–7.26	4.1	2.6	36.1	0.0246	0.0006
686.01	0	13.58	–4.36	3.5	0.1	96.8	0.0247	0.0000
693.01	0	13.95	–8.26	7.4	5.4	27.8	0.0244	0.0013
693.02	0	13.95	–8.09	7.0	4.9	29.6	0.0244	0.0012
695.01	0	13.44	–7.66	5.2	3.7	29.5	0.0251	0.0009
709.01	0	13.94	–7.57	6.6	4.2	36.8	0.0243	0.0010
717.01	0	13.39	–8.47	5.4	3.9	27.1	0.0251	0.0010
717.02	0	13.39	–9.90	8.4	6.9	17.3	0.0251	0.0017
739.01	0	15.49	–7.41	7.2	5.6	23.0	0.0256	0.0014
800.01	0	15.54	–7.22	24.2	19.3	20.3	0.0243	0.0047
800.02	0	15.54	–7.16	23.5	18.6	20.9	0.0243	0.0045
834.01	0	15.08	–5.84	6.8	2.9	57.4	0.0241	0.0007
834.02	0	15.08	–7.72	14.3	10.4	27.4	0.0241	0.0025
834.03	0	15.08	–8.35	17.4	13.5	22.5	0.0241	0.0033
834.04	0	15.08	–9.27	22.0	18.1	17.8	0.0241	0.0044
834.05	0	15.08	–8.11	16.2	12.3	24.2	0.0241	0.0030
884.01	0	15.07	–5.95	6.7	3.4	48.2	0.0242	0.0008
884.02	0	15.07	–6.02	6.9	3.7	46.6	0.0242	0.0009
884.03	0	15.07	–7.89	14.1	10.8	22.9	0.0242	0.0026
1096.01	0	14.71	–4.89	5.4	0.7	87.7	0.0234	0.0002
1174.01	1	13.45	–6.76	7.9	2.5	68.0	0.0252	0.0006
1236.01	0	13.66	–7.24	6.3	3.8	39.2	0.0246	0.0009
1236.02	0	13.66	–8.19	9.3	6.8	26.7	0.0246	0.0017
1236.03	0	13.66	–7.93	8.4	5.9	29.5	0.0246	0.0015
1268.01	0	14.81	–4.77	3.5	0.3	90.3	0.0239	0.0001
1353.01	0	13.96	–4.50	5.2	0.2	96.9	0.0235	0.0000
1353.02	0	13.96	–7.98	26.0	18.1	30.2	0.0235	0.0043
1356.01	0	15.21	–5.20	6.9	2.1	69.0	0.0240	0.0005
1421.01	0	15.30	–4.85	3.0	0.7	76.8	0.0250	0.0002
1426.01	0	14.23	–7.17	4.4	2.7	37.6	0.0246	0.0007
1426.02	0	14.23	–5.60	2.2	0.6	71.8	0.0246	0.0002
1426.03	0	14.23	–5.54	2.1	0.6	73.7	0.0246	0.0001
1452.01	1	13.63	–4.50	2.7	0.1	96.6	0.0246	0.0000
1477.01	0	15.92	–4.60	4.5	1.4	68.1	0.0256	0.0004
1529.01	0	14.31	–8.46	9.8	7.8	20.4	0.0241	0.0019
1529.02	0	14.31	–9.42	12.9	10.9	15.5	0.0241	0.0026
1546.01	1	14.46	–4.38	9.1	0.6	93.9	0.0226	0.0001
1596.01	0	15.16	–8.11	28.4	22.7	20.1	0.0237	0.0054
1596.02	0	15.16	–6.88	18.0	12.3	31.6	0.0237	0.0029
1684.01	0	12.85	–6.59	6.4	1.5	76.7	0.0283	0.0004
1701.01	0	11.04	–9.70	17.2	11.9	30.8	0.0453	0.0054
1725.01	1	13.50	–6.40	2.4	0.8	65.0	0.0250	0.0002
1779.01	0	13.30	–6.63	8.6	2.7	69.0	0.0259	0.0007
1779.02	0	13.30	–7.12	10.8	4.6	56.9	0.0259	0.0012
1781.01	1	12.23	–6.42	1.7	0.3	82.1	0.0292	0.0001
1781.02	1	12.23	–7.47	2.8	1.3	55.5	0.0292	0.0004
1781.03	1	12.23	–6.81	2.1	0.6	72.8	0.0292	0.0002
1800.01	0	12.39	–6.01	1.4	0.1	89.3	0.0280	0.0000
1802.01	1	13.35	–7.61	6.9	3.5	49.0	0.0254	0.0009
1805.01	0	13.83	–7.22	8.7	4.2	52.0	0.0242	0.0010
1805.02	0	13.83	–7.65	10.4	5.9	43.4	0.0242	0.0014
1805.03	0	13.83	–8.36	13.7	9.2	32.8	0.0242	0.0022

Table 7. continued.

Planet candidate	Type[a]	m_{kep} mag	Δm_{max} mag	$P_{BS,0}$ %	P_{BS}^{LB14} %	Improve %	P_{appEB} %	P_{BB} %
1894.01	0	13.43	–8.20	12.8	8.2	36.3	0.0253	0.0021
1925.01	0	9.44	–9.30	3.5	1.7	50.8	0.0490	0.0009
2042.01	0	13.09	–7.32	12.6	5.8	54.2	0.0271	0.0016
2133.01	0	12.49	–7.98	4.3	2.3	46.0	0.0283	0.0007
2260.01	0	12.17	–9.95	8.9	7.1	20.8	0.0303	0.0021
2324.01	1	11.67	–9.06	7.1	5.8	18.4	0.0351	0.0020
2352.01	0	10.42	–10.12	4.6	3.2	30.1	0.0409	0.0013
2352.02	0	10.42	–10.39	5.1	3.7	27.0	0.0409	0.0015
2352.03	0	10.42	–10.44	5.2	3.8	26.4	0.0409	0.0016
2545.01	0	11.75	–10.61	7.7	6.4	17.2	0.0312	0.0020
2593.01	0	11.71	–10.03	5.6	4.3	23.0	0.0306	0.0013
2632.01	0	11.39	–10.25	5.5	4.8	12.5	0.0323	0.0015
2640.01	0	13.23	–7.94	8.8	5.0	42.6	0.0259	0.0013
2674.01	0	13.35	–6.07	3.6	0.5	86.0	0.0254	0.0001
2674.02	0	13.35	–9.60	15.4	11.9	22.9	0.0254	0.0030
2674.03	0	13.35	–9.84	16.5	13.0	21.3	0.0254	0.0033
2712.01	0	11.12	–8.99	8.0	4.0	49.7	0.0419	0.0017
3179.01	0	10.88	–9.93	26.6	18.1	32.0	0.0486	0.0088
3203.01	0	11.82	–8.84	13.5	7.7	43.3	0.0371	0.0028
3206.01	0	11.84	–8.87	8.1	5.4	33.5	0.0345	0.0018
3237.01	0	12.32	–8.12	4.6	2.1	53.7	0.0294	0.0006
3444.01	1	13.69	–8.79	41.8	30.9	26.2	0.0242	0.0075
3444.02	1	13.69	–5.97	12.3	2.3	81.1	0.0242	0.0006
3444.03	1	13.69	–9.48	54.1	43.1	20.3	0.0242	0.0104
3554.01	0	15.21	–1.36	0.4	0.0	99.7	0.0246	0.0000
3560.01	0	11.82	–0.90	0.1	0.0	99.8	0.0376	0.0000
3728.01	0	12.25	–6.61	2.6	0.4	83.5	0.0304	0.0001
3742.01	0	14.96	–1.66	1.9	0.0	99.2	0.0228	0.0000
3765.01	0	16.44	–2.50	1.6	0.1	95.2	0.0263	0.0000
3801.01	0	16.00	–4.49	7.9	2.5	68.5	0.0251	0.0006
3853.01	0	10.63	–7.53	2.5	0.4	83.6	0.0437	0.0002
3890.01	0	13.23	–6.51	5.8	1.7	71.7	0.0261	0.0004
3925.01	0	14.03	–6.92	5.1	2.3	54.5	0.0242	0.0006
3925.02	0	14.03	–8.08	8.0	5.2	34.6	0.0242	0.0013
3925.03	0	14.03	–8.17	8.3	5.5	33.5	0.0242	0.0013
4016.01	1	14.07	–6.92	4.8	2.4	50.3	0.0243	0.0006
4351.01	0	15.00	–5.59	5.8	2.3	60.2	0.0241	0.0006
Demoted KOIs								
6.01	0	12.16	–8.13	14.3	8.3	42.1	0.0346	0.0029
1187.01	0	14.49	–6.44	10.6	4.7	55.6	0.0233	0.0011
1924.01	0	7.84	–10.29	4.7	3.2	32.9	0.0199	0.0006
3157.01	0	8.16	–9.70	1.3	1.0	22.1	0.0498	0.0005
3178.01	0	10.86	–6.40	2.1	0.1	93.2	0.0444	0.0001
3564.01	1	14.50	–1.51	0.2	0.0	99.2	0.0246	0.0000
3570.01	0	15.05	–1.66	1.2	0.0	99.5	0.0233	0.0000
3571.01	0	15.52	–0.91	0.7	0.0	99.7	0.0240	0.0000
3588.01	0	16.32	–0.83	0.6	0.0	99.8	0.0255	0.0000
3597.01	0	14.37	–2.47	1.7	0.0	99.5	0.0229	0.0000
3616.01	1	15.84	–3.65	7.6	1.3	82.8	0.0246	0.0003
3639.01	1	13.44	–3.63	1.8	0.0	98.2	0.0253	0.0000
3658.01	0	15.62	–3.71	5.8	0.0	100.0	0.0244	0.0000
3684.01	1	12.29	–2.57	0.2	0.0	99.0	0.0294	0.0000
3693.01	1	14.73	–5.60	9.8	3.3	66.0	0.0231	0.0008
3704.01	1	17.38	–1.51	2.2	0.1	97.1	0.0226	0.0000
3706.01	0	14.62	–0.52	0.2	0.0	100.0	0.0230	0.0000
3708.01	0	17.72	–0.74	2.5	0.0	99.8	0.0159	0.0000
3712.01	1	16.99	–1.99	2.8	0.1	97.0	0.0246	0.0000
3714.01	1	15.21	–4.71	4.4	0.9	79.4	0.0243	0.0002
3719.01	1	16.18	–3.49	4.2	1.0	76.5	0.0255	0.0003
3719.01	1	16.18	–3.49	4.2	1.0	76.6	0.0255	0.0003
3723.01	0	10.82	–6.66	4.5	3.0	34.2	0.0485	0.0014
3725.01	0	10.05	–6.67	2.6	0.3	89.3	0.0524	0.0001
3727.01	0	15.63	–5.37	8.0	3.3	59.1	0.0248	0.0008

Table 7. continued.

Planet candidate	Type[a]	m_{kep} mag	Δm_{max} mag	$P_{BS,0}$ %	P_{BS}^{LB14} %	Improve %	P_{appEB} %	P_{BB} %
3730.01	0	18.79	–0.84	1.9	0.8	56.4	-0.0023	-0.0000
3744.01	0	15.77	–4.91	6.6	2.2	66.9	0.0251	0.0005
3763.01	0	17.38	–0.68	0.9	0.0	100.0	0.0224	0.0000
3777.01	1	11.50	–7.52	9.0	1.9	78.8	0.0415	0.0008
3788.01	1	9.69	–8.87	3.1	1.2	60.7	0.0485	0.0006
3793.01	0	16.68	–3.26	3.0	0.6	81.6	0.0262	0.0001
3795.01	0	14.81	–0.76	0.3	0.0	99.9	0.0234	0.0000
3796.01	0	12.71	–6.80	5.8	1.6	72.7	0.0290	0.0005
3800.01	0	17.47	–3.48	7.0	4.2	40.1	0.0226	0.0009
3803.01	0	13.76	–6.61	8.0	2.6	67.6	0.0242	0.0006
3805.01	1	11.36	–4.77	1.3	0.0	96.3	0.0416	0.0000
3810.01	0	16.76	–3.48	2.8	0.8	72.7	0.0265	0.0002
3814.01	0	12.86	–7.33	11.1	5.1	54.2	0.0285	0.0014
3817.01	0	16.43	–4.54	15.7	6.3	59.7	0.0250	0.0016
3821.01	0	16.75	–4.03	6.9	2.5	63.3	0.0254	0.0006
3824.01	0	15.90	–5.26	8.2	3.8	53.8	0.0252	0.0010
3827.01	0	15.36	–5.35	14.8	5.6	62.0	0.0237	0.0013
3827.02	0	15.36	–5.41	15.2	6.0	60.4	0.0237	0.0014
3842.01	1	17.45	–0.87	1.0	0.0	100.0	0.0227	0.0000
3845.01	0	13.72	–6.36	6.0	1.4	75.9	0.0244	0.0004
3849.01	0	16.18	–4.03	4.4	1.1	73.9	0.0257	0.0003
3873.01	0	10.42	–5.55	0.7	0.0	94.6	0.0452	0.0000
3919.01	0	12.96	–7.68	8.5	3.8	55.0	0.0274	0.0010
3940.01	1	12.93	–7.31	11.0	4.0	63.9	0.0280	0.0011
3993.01	0	9.16	–7.99	1.3	0.9	32.5	0.0483	0.0004
3998.01	0	16.98	–4.28	18.7	9.0	52.2	0.0236	0.0021
4013.01	1	9.07	–10.63	6.5	5.5	16.6	0.0484	0.0026
4033.01	1	11.97	–7.18	3.0	0.7	76.7	0.0322	0.0002
4355.01	1	13.48	–7.83	17.9	9.8	45.3	0.0251	0.0025
4355.02	1	13.48	–7.85	18.1	10.0	44.9	0.0251	0.0025
4355.03	1	13.48	–7.57	16.0	7.9	50.7	0.0251	0.0020
4355.04	1	13.48	–8.10	20.2	12.1	40.2	0.0251	0.0030
4355.05	1	13.48	–7.38	14.8	6.7	54.8	0.0251	0.0017

Table 11. Comparison between the blended source probabilities (P_{BS}, in %) obtained by using the L13 (Law et al. 2013) and our high-resolution images (LB14) for coincident planet candidates (167 in total).

Planet candidate	$P_{BS,0}$ (%)	P_{BS} (%) L13	P_{BS} (%) LB14	Planet candidate	$P_{BS,0}$ (%)	P_{BS} (%) L13	P_{BS} (%) LB14	Planet candidate	$P_{BS,0}$ (%)	P_{BS} (%) L13	P_{BS} (%) LB14
12.01	1.80	0.0	0.7	416.02	6.90	5.9	4.1	709.01	6.60	5.2	4.2
41.01	6.10	4.6	1.9	416.03	15.50	14.5	12.7	717.01	5.40	4.6	3.9
41.02	10.10	8.5	5.8	431.01	4.00	2.9	2.4	717.02	8.40	7.7	6.9
41.03	9.40	7.9	5.2	431.02	4.50	3.4	2.9	739.01	7.20	5.3	5.6
49.01	8.10	7.1	3.4	435.01	5.80	4.9	3.3	800.01	24.20	20.6	19.3
69.01	4.10	3.1	1.5	435.02	2.60	1.6	0.3	800.02	23.50	20.0	18.6
82.01	1.30	0.6	0.2	435.03	8.50	7.5	5.9	834.01	6.80	5.1	2.9
82.02	2.50	1.8	1.0	435.04	11.50	10.5	8.9	834.02	14.30	12.6	10.4
82.03	3.10	2.4	1.6	435.05	7.40	6.4	4.9	834.03	17.40	15.7	13.5
82.04	4.20	3.5	2.7	435.06	12.30	11.3	9.7	834.04	22.00	20.3	18.1
82.05	5.30	4.6	3.8	463.01	17.90	10.7	9.0	834.05	16.20	14.5	12.3
94.01	3.70	1.9	0.3	478.01	10.20	2.5	6.0	884.01	6.70	5.1	3.4
94.02	10.60	8.8	4.1	481.01	10.10	7.5	7.0	884.02	6.90	5.3	3.7
94.03	6.80	5.0	1.2	481.02	13.80	11.1	10.6	884.03	14.10	12.5	10.8
94.04	23.80	22.0	17.2	481.03	9.70	7.1	6.6	1230.01	4.10	0.02	0.2
111.01	5.40	4.5	2.3	528.01	7.50	6.6	5.3	1236.01	6.30	5.5	3.8
111.02	5.60	4.7	2.6	528.02	6.60	5.6	4.3	1236.02	9.30	8.5	6.8
111.03	4.90	4.1	1.9	528.03	7.40	6.5	5.2	1236.03	8.40	7.6	5.9
111.04	13.00	12.1	9.9	534.01	19.10	14.7	14.3	1353.01	5.20	0.8	0.2
115.01	4.50	3.7	1.9	534.02	24.00	19.6	19.2	1353.02	26.00	21.6	18.1
115.02	7.40	6.6	4.8	561.01	5.80	4.7	4.2	1426.01	4.40	3.3	2.7
115.03	14.80	13.9	12.2	564.01	21.90	19.3	15.6	1426.02	2.20	1.1	0.6
139.01	3.90	3.0	0.9	564.02	9.70	7.1	3.5	1426.03	2.10	1.0	0.6
139.02	15.20	14.3	12.0	564.03	35.60	33.0	29.3	1452.01	2.70	0.4	0.1
149.01	6.00	5.3	2.6	567.01	12.70	9.9	8.6	1529.01	9.80	6.3	7.8
152.01	13.60	10.9	3.3	567.02	14.70	11.9	10.6	1529.02	12.90	9.4	10.9
152.02	25.10	22.4	14.4	567.03	13.80	10.9	9.7	1596.01	28.40	25.5	22.7
152.03	26.60	24.0	16.0	571.01	28.10	14.0	20.1	1596.02	18.00	15.1	12.3
152.04	31.30	28.7	20.7	571.02	26.00	11.8	17.9	1684.01	6.40	1.9	1.5
156.01	9.90	5.5	6.2	571.03	32.40	18.2	24.4	1701.01	17.20	14.7	11.9
156.02	12.40	8.0	8.7	571.04	27.90	13.7	19.8	1725.01	2.40	1.6	0.8
156.03	6.70	2.4	3.0	571.05	33.20	19.1	25.2	1779.01	8.60	7.4	2.7
191.01	6.80	3.4	0.8	579.01	10.70	8.9	7.8	1779.02	10.80	9.6	4.6
191.02	28.00	24.6	21.5	579.02	10.50	8.8	7.7	1781.01	1.70	0.4	0.3
191.03	43.50	40.1	36.9	611.01	11.80	6.1	2.9	1781.02	2.80	1.5	1.3
191.04	28.20	24.8	21.6	624.01	10.80	8.5	5.2	1781.03	2.10	0.7	0.6
209.01	2.80	1.2	0.6	624.02	11.00	8.7	5.3	1802.01	6.90	5.6	3.5
209.02	4.30	2.7	1.9	624.03	17.70	15.4	12.1	1805.01	8.70	6.6	4.2
211.01	3.10	1.9	0.6	625.01	5.70	4.2	3.2	1805.02	10.40	8.3	5.9
238.01	23.90	19.5	16.4	632.01	13.00	11.3	9.9	1805.03	13.70	11.7	9.2
238.02	39.00	34.6	31.5	638.01	15.20	11.5	8.8	1812.01	7.30	5.3	3.1
330.01	16.30	10.7	11.9	638.02	14.60	11.0	8.3	1894.01	12.80	8.3	8.2
330.02	29.00	23.3	24.6	640.01	21.10	19.2	10.8	1924.01	4.70	4.4	3.2
339.01	7.10	6.0	5.1	650.01	8.60	6.7	7.4	1925.01	3.50	3.0	1.7
339.02	7.20	6.1	5.2	654.01	8.40	7.0	6.5	2042.01	12.60	11.3	5.8
339.03	7.40	6.3	5.4	654.02	9.10	7.7	7.1	2133.01	4.30	3.7	2.3
345.01	3.30	2.4	2.2	659.01	15.20	13.1	10.0	2260.01	8.90	7.5	7.1
349.01	5.10	2.8	3.2	664.01	15.80	13.8	11.8	2352.01	4.60	4.0	3.2
366.01	2.40	0.04	0.7	664.02	21.50	19.5	17.5	2352.02	5.10	4.5	3.7
372.01	4.20	0.01	0.8	664.03	21.20	19.3	17.3	2352.03	5.20	4.7	3.8
385.01	19.00	16.4	16.1	676.01	5.50	0.2	2.0	2481.01	16.60	13.1	10.0
386.01	16.70	14.7	9.9	676.02	7.40	1.9	3.8	2545.01	7.70	6.7	6.4
386.02	18.90	16.9	12.0	682.01	5.80	2.6	0.8	2593.01	5.60	4.8	4.3
388.01	8.40	7.1	6.1	684.01	4.10	3.1	2.6	2632.01	5.50	4.7	4.8
393.01	23.60	22.0	17.4	686.01	3.50	0.3	0.1	2640.01	8.80	7.3	5.0
416.01	6.00	5.0	3.1	695.01	5.20	4.2	3.7				